Environmental Modelling and Software 197 (2026) 106822

Contents lists available at ScienceDirect

Environmental Modelling and Software

journal homepage: www.elsevier.com/locate/envsoft

PMAR: A Lagrangian approach to the modelling of anthropogenic pressures for marine management

Sofia Bosi [a,b,*], Alessandra Raffaetà [b], Marta Simeoni [b,c], Nikola Bobchev [d], Dimitar Berov [d], Andrea Barbanti [a], Stefano Menegon [a]

[a] Insitute of Marine Sciences (ISMAR) of the National Research Council of Italy (CNR), Castello 2737/F, Venice, 30122, Italy
[b] Department of Environmental Sciences, Informatics and Statistics, Università Ca' Foscari Venezia, Via Torino 155, Venice, 30172, Italy
[c] European Centre for Living Technology (ECLT), Dorsoduro 3911, Venice, 30123, Italy
[d] Institute of Biodiversity and Ecosystem Research, Bulgarian Academy of Sciences, 2 Yuri Gagarin Street, Sofia, 1113, Bulgaria

ARTICLE INFO

Keywords:
Lagrangian trajectories
Python
OpenDrift
Pressure assessment
Cumulative Effects Assessment
Maritime Spatial Planning
Scenario analysis

ABSTRACT

PMAR (Pressure models for MARine activities) is a modelling framework and open-source Python-based software designed to assess anthropogenic pressures for marine management. PMAR uses Lagrangian trajectories calculated from ocean models to simulate pressure dispersion. An explicit link between pressures and their sources is established through a weight-based mechanism, which allows to rapidly explore different pressure source scenarios. Here, PMAR is adopted to investigate the distribution of surface macroplastics in the Black Sea under two scenarios, yielding results consistent with previous modelling studies and observations. Over 50% of the macroplastics in each Black Sea country after a yearly run came from elsewhere, stressing the importance of cross-boundary cooperation. Compared to other pressure modelling frameworks, PMAR emerges as a balanced compromise between computational efficiency and predictive accuracy. Future work will focus on making PMAR accessible to decision-makers and aligning it with requirements of Digital Twin of the Ocean applications.

Software availability

- Name of software: PMAR
- Developers: Sofia Bosi and Stefano Menegon
- Contact: sofiabosi@cnr.it and stefano.menegon@cnr.it
- Date first available: 22 April 2025
- Software required: OpenDrift v1.14 and rioxarray v0.19
- Program language: Python
- Source code at: https://github.com/CNR-ISMAR/pmar
- Documentation: Installation instructions can be found in https://github.com/CNR-ISMAR/pmar/blob/main/README.md, while the source code contains documentation on specific classes and methods.

1. Introduction

The marine environment contains a pool of resources that human life both depends on and benefits from. However, these resources are finite and are increasingly threatened by continuous exploitation (European Ocean Pact stakeholder group, 2024). In response to growing awareness on the consequences of the mismanagement of marine resources, policy makers have introduced regulatory frameworks for sustainable management, such as Maritime Spatial Planning (MSP).

In Europe, MSP is governed by the Maritime Spatial Planning Directive (MSPD, Directive 2014/89/EU, Council of the European Union, European Parliament (2014)). The MSPD explicitly requires Member States, when drafting their Maritime Spatial Plan, to: consider the impacts of human activities on the marine environment (Art. 4); adopt an Ecosystem-Based Approach (EBA) to balance ecological, economic, and social objectives (Art. 5); establish means for public participation from the early stages in the development of the MSP (Art. 9); use the best available environmental, social, and economic data (Art. 10); and ensure trans-boundary cooperation (Art. 11).

An essential practice of EBA in MSP is the Cumulative Effects Assessment (CEA), which evaluates the combined effects of multiple human activities and natural processes on the environment (Hammar et al., 2020). CEA is a specific form of Environmental Impact Assessment (EIA) that focuses on holistic cross-sectoral evaluations, rather than isolated activity-based assessments (Jones, 2016).

* Corresponding author at: Insitute of Marine Sciences (ISMAR) of the National Research Council of Italy (CNR), Castello 2737/F, Venice, 30122, Italy.
E-mail address: sofiabosi@cnr.it (S. Bosi).

https://doi.org/10.1016/j.envsoft.2025.106822
Received 22 April 2025; Received in revised form 7 November 2025; Accepted 4 December 2025
Available online 5 December 2025

Various methodologies have been developed in recent years to operationalise CEA, including EcoImpactMapper (Stock, 2016), CEA Tools4MSP (Menegon et al., 2018a,c), Mytilus (Hansen, 2019), PlanWise4Blue (Kotta et al., 2020), Spatial Pressures and Impact Assessment - SPIA (HELCOM, 2019), and Symphony Sweden (Hammar et al., 2020). These approaches are easy to interpret for planners, stakeholders, and policy makers (Hammar et al., 2020) and have been widely adopted. Most existing CEA tools for MSP are based on the framework first introduced by Halpern (Halpern et al., 2008), which uses geospatial indices to model how human activities generate pressures and impact ecosystem components.

An MSP-oriented CEA typically requires the analysis of large geographically referenced datasets, as planners must consider multiple ecological components, human activities, and associated pressures, including land-based sources (Hammar et al., 2020; Lonsdale et al., 2020). An effective CEA should aim to model the "impact chain" in a spatially explicit manner. Understanding *Activity – Pressure – Pathway – Receptor* relationships (Judd et al., 2015) is crucial to design successful planning measures, which target the sources of pressures, i.e., economic maritime activities such as shipping, coastal tourism, offshore energy infrastructure, fisheries and aquaculture (Judd et al., 2015; Fernandes et al., 2017; Menegon et al., 2018a; Willsteed et al., 2018; Farella et al., 2021; Stelzenmüller et al., 2024; Bosi et al., 2023). Moreover, an explicit representation of these relationships within CEA enables scenario-based MSP, that is, it allows planners to evaluate alternative spatial configurations of human activities, or "what-if scenarios" (Menegon et al., 2018b; Farella et al., 2020; Hammar et al., 2020; Stelzenmüller et al., 2024).

However, existing tools are often quite rudimentary in modelling the different steps of the impact chain, particularly the *Activity – Pressure* link (pressure modelling). Anthropogenic pressures, or stressors, are defined by the Marine Strategy Framework Directive (MSFD, Council of the European Union, European Parliament, 2008) as events or agents (biological, chemical or physical) exerted by anthropogenic sources that elicit a harmful effect on environmental receptors (Judd et al., 2015). The simplest modelling approach equates stressors with the mere presence of human activities, without explicitly simulating pressure dispersion or propagation mechanisms (Halpern et al., 2008). Other methodologies use isotropic buffers of varying distances to approximate the spatial extent of pressures, or apply a linear or Gaussian decay from the source (Korpinen et al., 2012; Heinänen et al., 2013; Stock and Micheli, 2016; Menegon et al., 2018a).

Although these approaches may be suitable for certain local pressures, they often result in high uncertainty (Stock and Micheli, 2016; Gissi et al., 2017) or are completely unrealistic (Judd et al., 2015). This is particularly true for substances that exhibit anisotropic dispersion and are thus affected by ocean currents, waves, winds, and biogeochemical processes (e.g., marine litter, nutrients, etc.), and whose variability cannot be captured unless ocean and atmospheric data are explicitly involved in the modelling.

External, bespoke pressure layers produced by specialised models (e.g., the Spatial Distribution of Pressures and Impacts developed within the HOLAS III assessment, HELCOM (2023)) are sometimes used as the best available data. However, while adopting output of specialised models may improve the accuracy of CEA results, incorporating external models leads to the loss of explicit connections between the *Activity* and *Pressure* components of the impact chain, i.e., between the pressure and its source.

In this study, a new framework and software called *Pressure models for MARine activities* (*PMAR*) is proposed to model and assess the propagation of anthropogenic pressures at sea from different human activities. PMAR captures the "dynamic realism" of the marine environment by simulating pressures as the dispersal of Lagrangian particles (Halpern et al., 2009). Extensive scientific literature is available on the use of Langrangian particle tracking algorithms to study the transport of oil spills (Goeury et al., 2014), marine litter (Zambianchi et al., 2017), macro- and microplastics (Tsiaras et al., 2021), chemicals (Aghito et al., 2023), fish larvae (McDonald and Nelson, 2021), resuspended sediment (Baharvand et al., 2023) and water parcels (Ricker and Stanev, 2020).

Employing Lagrangian Particle Tracking (LPT) algorithms for pressure modelling ensures a more realistic representation than a simple decay of the pressure from the source. For instance, it is known that some pressures may be minimised at the source or produce effects that occur far away from the site of the activity, due to the dynamic nature of the marine environment (Elliott et al., 2020). Trajectories resulting from LPT algorithms are calculated from ocean models, thus capturing ocean dynamics and potential transboundary effects. In addition, as LPTs compute the full trajectory within a given time, the connection between the pressure and its source remains explicit in PMAR. This is crucial from an EBA perspective (Judd et al., 2015), since management occurs at the activity (and not at the pressure) level (Elliott et al., 2020).

Next, as one pressure may come from a variety of sources (e.g., marine litter may be released by coastal cities, or shipping, or river runoff), PMAR exploits a weight-based mechanism to quickly explore dispersal from different human activities. To achieve this, trajectories are given a weight that represents the amount of pressure being transported by each trajectory and that depends on the location and intensity of the source. In this configuration, particles do not represent one single object, but can rather be thought of as Super Individuals (Scheffer et al., 1995), i.e. a cluster of particles with similar characteristics.

Finally, PMAR's output is designed to be compatible with the spatial analysis carried out in the MSP process and the analysis of cumulative impacts (such as e.g. Hammar et al. (2020)). Pressure propagation is thus represented on a geo-referenced map showing an Index of Pressure Propagation (*PPI*), obtained by calculating the weighted sum of all trajectories passing through a cell of the grid during the time of the analysis. By assigning weights to pre-calculated trajectories, and thinking of a virtual particle as a cluster of objects or amount of a substance whose magnitude is given by the weight, it is possible to explore different pressure source scenarios "on-demand".

The aim of this work is to present the methodology of the PMAR framework, and demonstrate its value as a trade-off between the accuracy and flexibility of existing methodologies for pressure modelling and assessment. We investigate the propagation of surface macroplastics in the Black Sea to showcase the applicability of the tool. We validate the result against observational data and compare with other existing models through a "toy problem". Finally, we discuss advantages and limitations of PMAR in modelling different types of pressures.

2. Methods

PMAR operates in a sequence of steps, shown in Fig. 1. The model requires two types of data inputs: (i) ocean and atmospheric velocity fields, and (ii) maps of human activities at sea, i.e., the pressure sources. From the first set of inputs, a series of trajectories are created by following the paths traced by virtual particles in seawater. These particles can be configured with different physical characteristics to represent different substances (pressures).

The spatial distribution of a human activity in the region of interest (the second input) is then used to assign weights to the trajectories based on their starting position, thus creating a spatial correlation between the pressure and its source. In particular, the weights are a function of the intensity of the human activity in the starting position of each trajectory (see Section 2.3 for a more detailed explanation). Finally, the trajectories are aggregated to return a map of pressure propagation. We call the value associated to each cell in the map the Pressure Propagation Index, or *PPI*.

The motivation behind this framework and its objectives are outlined in Section 2.1. The structure of the PMAR software is presented in Section 2.2 and the methodology used to assign weights to trajectories and calculate the *PPI* is detailed in Section 2.3. The case study area is described in Section 2.4, followed by Section 2.5 detailing the experimental design and Section 2.6, on the software implementation.

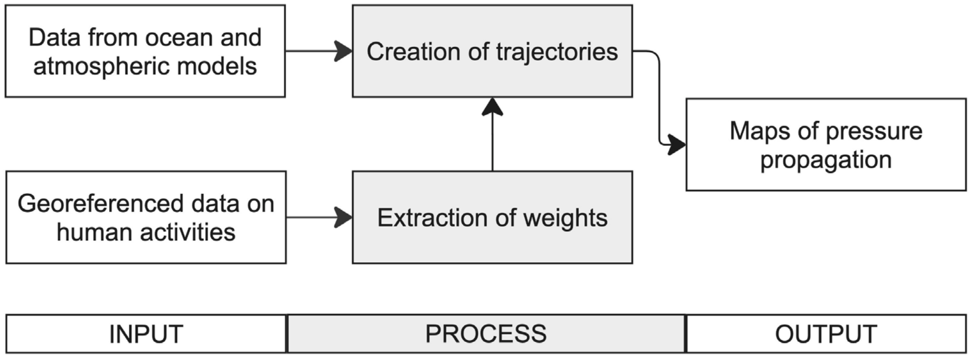

Fig. 1. The core of the PMAR workflow, which calculates trajectories of virtual particles forced by ocean and atmospheric models, then assigns them weights extracted from maps of human activities, and finally produces maps of pressure propagation.

2.1. The PMAR framework

The PMAR framework is developed to be fully oriented to Ecosystem-based management and Maritime Spatial Planning. This means, in the authors' view, that the following needs have to be met: (i) being able to model the propagation of multiple pressures, (ii) accomodating various spatio-temporal domains and scales, (iii) generating quantitative and spatially explicit outputs, (iv) linking the modelled pressures to their sources.

The first objective is achieved by exploiting Lagrangian Particle Tracking algorithms (LPT). Some pressures, in particular those defined as "substances", "litter" or "agents" in the MSFD and in Judd et al. (2015), act as transient tracers in seawater (Talley, 2011). Their transport can thus be simulated using LPT (Van Sebille et al., 2018). Such algorithms follow virtual particles transported by velocity fields in seawater, and return trajectories. By changing parameters related to the physical characteristics of the particles, such as density, size, or sinking velocity, the user is able to simulate the motion of different objects or substances.

Secondly, the flexibility to perform the analysis in different spatio-temporal domains and scales is accomplished by taking advantage of the data publicly accessible via the Copernicus Marine Data Store.[1] PMAR is able to remotely access the various wind and ocean current velocity fields available on the portal, at the global or basin scale, and use them to force particle movement. The user only needs to specify the name of the desired ocean basin, or the coordinates of a sub-area, and the relevant data is loaded automatically, as long as Copernicus credentials are provided for authentication.

Third, as the spatial aspect is essential to support marine management and, of course, spatial planning, PMAR's primary outputs are provided in the form of maps. Maps are obtained by subdividing the area of interest into a regular spatial grid of user-defined resolution, and binning trajectories onto this grid. Maps are then georeferenced and saved as a raster file, i.e. the format typically used by tools performing spatial analyses informing MSP like Cumulative Effects Assessment (CEA) (see e.g. Depellegrin et al. (2021) for a review of existing tools). Moreover, the resolution and bounds of the spatial domain are fully customisable, allowing the user to perform analyses at different scales and respond to different management questions.

Finally, it is crucial to explicitly link pressures to their sources for transparency in the impact chain. To accomplish this, a map of either the intensity or presence of a human activity (or "use") in the region of interest may be provided as input to PMAR. To each trajectory, the tool assigns a weight that is based on the value of the use in the location where the trajectory was released. The weighted sum of all trajectories crossing a cell during the time of the analysis is then associated to each cell. This value represents the *PPI*.

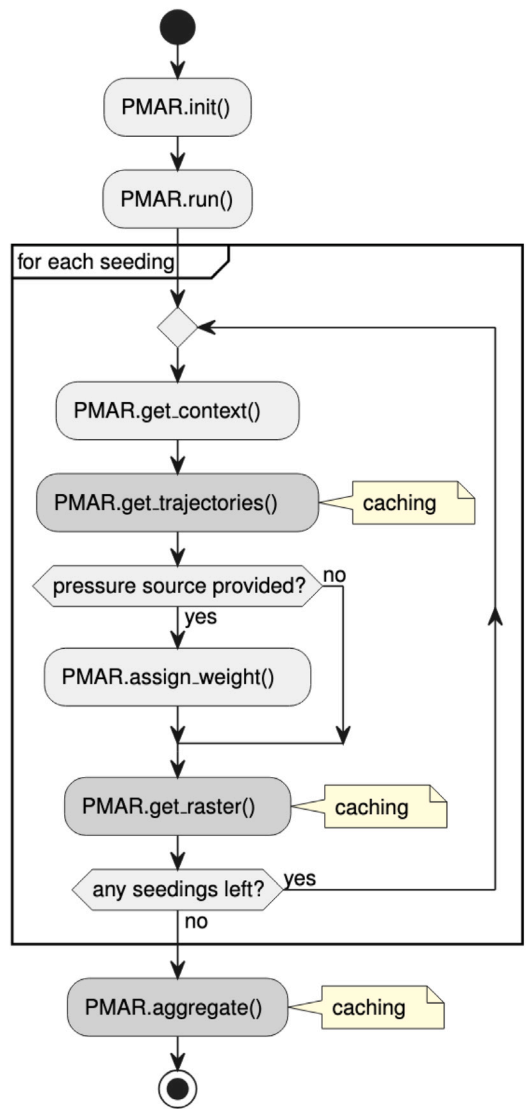

Fig. 2. Activity diagram showing the flow of the PMAR class within the PMAR software. The diagram uses an object-oriented syntax (*class.method()*). "If" statements are enclosed by diamonds, while the box indicates a "for loop" that is carried out for each seeding.

[1] https://data.marine.copernicus.eu

2.2. Software architecture

The current version of the PMAR software v0.15 comprises two core classes, `PMAR` and `PMARCache`: the first is used to produce results, the second to store output files and their metadata in a cache directory. The activity diagram in Fig. 2 shows the general workflow of class `PMAR`.

After instancing the `PMAR` object, method `PMAR.run()` launches three consecutive steps: (i) calculation of trajectories, (ii) rasterisation, and (iii) aggregation, corresponding to methods `PMAR.get_trajectories()`, `PMAR.get_raster()`, and `PMAR.aggregate()` in the diagram, respectively. After each step, PMAR writes the corresponding output files to a cache directory (`caching` comment in Fig. 2). The `PMARCache` class then, at each step, checks whether a file with the same metadata already exists in the cache directory to avoid unnecessary computation (not shown in figure for readability).

Steps (i) and (ii) occur in a loop for each seeding. A "seeding" is a uniquely identifiable ensemble of trajectories with the same start time and duration. Particles are released in multiple separate seedings and then aggregated (step iii). This way, a high (statistically significant) number of trajectories is created without overloading computer memory. We found that a maximum of 10^3 trajectories per seeding works well on a machine with 30 GB RAM and 12CPUs. Seedings can also be released at different times to simulate a continuous source. In this case, the user is required to specify the start time of the first seeding and a (fixed) time interval between consecutive seedings.

The loop starts by creating each requested set of trajectories (the seedings) and writing them to cache. Two methods are used to produce trajectories: `PMAR.get_context()` and `PMAR.get_trajectories()`. The first is used to pull the oceanic and atmospheric data needed for the particle simulation. These data can be provided either as a path to local files or simply as a string referring to the ocean basin of interest. In the latter case, PMAR connects to the Copernicus Marine Data Store and reads the relevant variables, provided that Copernicus credentials have been specified for authentication. Once the velocity data have been incorporated, method `PMAR.get_trajectories()` configures and launches OpenDrift (Dagestad et al., 2018) to calculate the trajectories. Trajectories are provided as NetCDF (Network Common Data Form) files containing the position of each virtual particle, in latitude and longitude coordinates, at each time step.

After writing the trajectory file into the cache folder, PMAR checks whether a file describing the intensity or presence/absence of a human activity in the area of interest was given. This human activity represents the pressure source. If a pressure source file is provided, weights are extracted from it and assigned to each trajectory with method `PMAR.assign_weight()`. Weights are calculated as a function of the pressure source map at the starting position of each trajectory and are constant along the trajectory, unless a decay rate is defined. This weight-based mechanism allows for the testing of various scenarios, i.e., different human activities acting as the source of the pressure, without having to recalculate trajectories for each source, thus keeping computational time to a minimum. Further details on the calculation of weights are given in Section 2.3.

To conclude the loop, `PMAR.get_raster()` bins the trajectories onto a spatial grid of user-defined resolution and produces a two-dimensional map. In particular, the weights of all trajectories found in each grid cell at each time step are added together, and then integrated over time, effectively removing the time dimension. Geographical information such as the Coordinate Reference System (CRS) and spatial resolution are included before rasterising the map onto a GeoTIFF image (Geographic Tagged Image File Format) and writing it into the cache directory.

After a raster file has been cached for every seeding, the loop ends, and method `PMAR.aggregate()` combines the rasters to produce the Pressure Propagation Index (*PPI*) map. The methodology used to aggregate different seedings is described in Section 2.3.

2.3. Rasterisation and aggregation

PMAR is designed to support marine management and spatial planning; therefore, as mentioned above, it outputs maps. To achieve this, the study area is partitioned onto a regular grid of square spatial cells whose resolution is defined by the user and where each cell is uniquely identifiable by a number c. Next, the weighted sum of all trajectories passing through a cell during the time of the analysis is associated to it. This process is carried out for each seeding and the aggregation of these results yields the Pressure Propagation Index (*PPI*).

Seedings are sets of trajectories released at the same time and with the same duration. They are identified by a numerical id and referred to as S_k, indicating the kth seeding. Trajectories (generated by PMAR method `PMAR.get_trajectories()`) are a sequence of spatio-temporal points with a fixed sampling rate, called *time step*. This value provides the time interval at which to continuously record positions in the spatial domain, and it is chosen by the user according to the spatial scale and resolution of the grid of analysis and on the characteristic time scales of the atmospheric and oceanic features in the basin of interest.

Let K be the number of seedings, τ be the constant time interval between two consecutive seedings, t_0 be the start time of the first seeding S_1 and T its duration. Note that all durations are expressed in terms of number of timesteps, including T and τ. Then, each seeding, S_k with $k = 1, \dots, K$, is released at time:

$$t^k_{start} = t_0 + (k-1) \cdot \tau \tag{1}$$

and has duration:

$$d_k = T - (k-1) \cdot \tau \; . \tag{2}$$

Notice that S_1, with duration $d_1 = T$, is the longest seeding, and its duration determines the duration of the run. The duration of each seeding after S_1 is obtained by subtracting multiples of τ. The sum of all durations, called γ, can thus be expressed as:

$$\gamma = \sum_{k=1}^{K} d_k = \sum_{i=0}^{K-1} (T - i \cdot \tau) \tag{3}$$

For each seeding, trajectories are rasterised as follows. First, they are binned using the grid mentioned above, so that each position, originally expressed with a pair of geographical coordinates, is now mapped onto the corresponding grid cell c. A trajectory p can thus be defined as a function $x_p : \mathbb{T} \to \mathbb{N}$ which, given a time instant t, returns the unique id of the cell (or bin) c the trajectory p is crossing at time t. The domain $\mathbb{T}$ is defined as the set of all time instants sampled from t_0 onward, at intervals of the selected time step, up to $t_{end} = t_0 + T - 1$ (independent of k). Recall that the trajectories belonging to the same seeding S_k start at the same time instant t^k_{start}. Given a trajectory $p \in S_k$, we thus denote with $c_p = x_p(t^k_{start})$ the cell where trajectory p starts.

Next, trajectories are assigned a weight based on the pressure source, here called U, for "use". U is a map of either the intensity or presence of a human activity, given by the user as input to the model. For consistency, the use map U is re-projected onto the same grid as the trajectories. It is worth remarking that the map of the pressure source may be fixed or may vary in time, depending on data availability. In the latter case, a different U is associated to each seeding, depending on the seeding's start time. Hence, we denote with $U^k(c)$ the value of the pressure source in cell c for the kth seeding.

Method `PMAR.assign_weight()` assigns weights to trajectories in seeding S_k based on three factors: the starting cell of each trajectory c_p, the pressure source value in that cell, $U^k(c_p)$, and the number of trajectories seeded within c_p. Specifically, the weight $w^k_p(t)$ of trajectory p in seeding S_k is defined as:

$$w^k_p(t) = \frac{d(t) \cdot f(U^k(c_p))}{\sum_{j \in S_k} \delta(c_j, c_p)} \qquad \text{for } t \in \mathbb{T} \wedge t \geq t^k_{start} \tag{4}$$

Function f, when present, converts the intensity of the use into the emission of a substance. For example, if U represents the number of vessels in a cell, $f(U)$ may return the amount of oil, in kg, released per time period per vessel. Moreover, as some substances degrade over time, the weight is multiplied by an exponential decay function $d(t) = e^{-\theta t}$, where decay coefficient θ is user-defined. The default value is $\theta = 0$ to represent no decay. In this case, the weight is constant in time, i.e., along the entire trajectory. Finally, w_p^k is normalised by the number of all trajectories belonging to seeding S_k that are released in the same cell as p (denominator of Eq. (4)). To compute this number we use function δ, which returns 1 if the input cells are equal, and 0 otherwise:

$$\delta(c_1, c_2) = \begin{cases} 1 & \text{if } c_1 = c_2 \\ 0 & \text{otherwise.} \end{cases} \tag{5}$$

This normalisation is made to ensure that the output raster is independent of the number of trajectories, provided that at least one trajectory is seeded in each cell of the grid. It implies that $U^k(c)$ (i.e., the use intensity in cell c for seeding S_k) is equally divided between the trajectories in S_k starting from cell c, and this fraction is the (initial) weight of these trajectories. In other words, the sum of all trajectory weights in cell c at start time t^k_{start} is equal to the value of the pressure source in that cell, $U^k(c)$. Therefore, if the use map is the constant function $U^k(c) = 1$, and there is neither function f nor decay d, the sum of the weights in all cells equals the total number of cells in the grid.

Next, method `PMAR.get_raster()`, aggregates the weights of the trajectories within each grid cell at every time instant $t \in \mathbb{T}$, and then integrates them over time. This operation is performed separately for each seeding. Formally, for each S_k with $k = 1, \dots, K$, and cell c, we define:

$$W^k(c) = \sum_{t \in \mathbb{T} \wedge t \geq t^k_{start}} \; \sum_{p \in S_k \wedge x_p(t) = c} w_p^k(t) \tag{6}$$

The time dimension is removed, and, for each seeding S_k, the output is a two-dimensional map, W^k, with aggregated weights.

The final step, implemented by method `PMAR.aggregate()`, combines the maps from all seedings to produce the final output of PMAR, the *Pressure Propagation Index* (*PPI*), defined in each cell c as:

$$PPI(c) = \frac{1}{\gamma} \sum_{k=1}^{K} W^k(c) \tag{7}$$

To ensure that the *PPI* is independent of the temporal resolution of the trajectories, the cell-weight is normalised by the number of time steps in each seeding. If all seedings had the same duration d, it would suffice to divide by $K \cdot d$. However, since different seedings may have different durations, we obtain this result by dividing by γ when aggregating multiple seedings. Note that, while d_k may vary, the time step is constant for all seedings.

The resulting map gives an indication of the pressure's propagation from the source in a given time span, assuming that the pressure is transported like a passive tracer in seawater.

2.4. Case study area

The Black Sea is a semi-enclosed basin with a surface area of 423000 km^2 and a maximum depth of 2200 m, with narrow shelves around the basin (BSC, 2019). The prevailing circulation of the surface layer is the cyclonic Rim Current, which causes cold upwelling in the interior. The Rim Current reaches its highest speeds along the Anatolian coast (Turkey) and south of Crimea. These features are visible in Fig. 3(a), which depicts the mean annual surface currents for the year 2019 from EU CMEMS-MDS (2024a). During the summer months, the Rim Current splits into two branches along the central part of the basin forming two distinct cyclonic gyres, one in the West and one in the East (Miladinova et al., 2020). In addition, a number of mesoscale eddies develop at the edge of the Rim Current with strong seasonal variations. Of these, the anticyclonic Batumi eddy is visible in Fig. 3(a) at around 40°E .

Mean annual surface wind speeds for the year 2019 are shown in Fig. 3(b). The Black Sea is characterised by prevailing northerly winds, whose direction diverges horizontally along the centre of the basin. On average, the strongest wind speeds (over > 2.5 m/s) of 2019 were recorded in the south-western region, close to the Bosphorus strait, and the lowest (< 0.5 m/s) near the Georgian coast. The surface wind is one of the main drivers of the general circulation in the Black Sea, together with the steep topography and the significant freshwater input from rivers, particularly the Danube (Miladinova et al., 2020).

While having a river catchment area of over $2.5 \cdot 10^6$ km^2 (BSC, 2007) on the territory of 23 European and Asian countries, the Black Sea is connected with the Mediterranean Sea only through the narrow Bosphorus channel, thus accumulating the inflow of silt, nutrients, organic matter, persistent organic pollutants, and floating marine litter, including macro and microplastics. As a result, its concentration of floating marine litter, 95% of which is plastic, is estimated to be three times higher than in the Mediterranean (González-Fernández et al., 2022). The Danube River alone contributes a total of 532.4 tonnes of macroplastics per year (Van der Wal et al., 2015), while the annual influx of plastic items smaller than 5 mm amounts to 1533 tonnes (Lechner et al., 2014).

Macroplastics are a significant source of microplastics (1 – 5000 μm) and nanoplastics (< 1 μm), as they gradually fragment into smaller pieces under physical and chemical stress in the marine environment (Kale et al., 2007; Andrady, 2015). In a recent monitoring study on microplastics in the Bulgarian Black Sea, fragments emerged as the most abundant class of microplastics (Berov and Klayn, 2020). Considering that microplastics are near impossible to remove from the water column and sediment, where they have also been found (Terzi et al., 2022; Bobchev et al., 2024), similar results highlight the importance of prevention measures aimed at larger plastic items to inhibit production at the source.

2.5. Experimental design

The aim of this first application of PMAR was to simulate the propagation of surface macroplastics in the Black Sea basin. While the expression "marine plastic" encompasses a wide range of objects with varying sizes and physical properties, the focus here was on highly buoyant plastic items larger than 5 mm. This allowed us to limit the analysis to the surface ocean and neglect, for now, the sinking of particles to the ocean floor.

Two case studies were tested: one where no human activity (or use) was specified as the pressure source, called *NoUse*, and one where the pressure source was maritime transport, called *ShippingUse*. While shipping has been identified as a significant source of marine litter (Novac et al., 2020; Lebreton et al., 2018), it is very difficult to monitor through *in situ* observations, as it is not straightforward to determine whether a piece of plastic found at sea was released by a ship or at land. Moreover, existing studies on marine plastic in the Black Sea mainly focus on rivers or coastal cities as sources (Miladinova et al., 2020; Stanev and Ricker, 2019). Macroplastic from shipping was therefore chosen here as an interesting subject for a modelling case study.

The emission function f was the identity function in both *NoUse* and *ShippingUse*, as no data was found at the time of writing on the amount of macroplastics released by shipping vessels in the Black Sea. The experiment was carried out in the three steps described in Section 2.2: (i) creation of trajectories, (ii) rasterisation and (iii) aggregation of results.

First, 10000 particles were released every $\tau = 3.65$ days for a year, starting from the 1st of January 2019. A duration of one year falls within what has been recognised as an informative timescale for the Black Sea, given the high speed of currents and the high

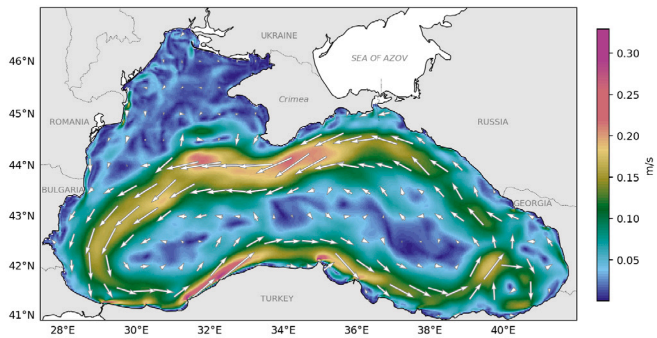

(a) Black Sea mean surface currents for the year 2019 (from EU CMEMS-MDS (2024a)).

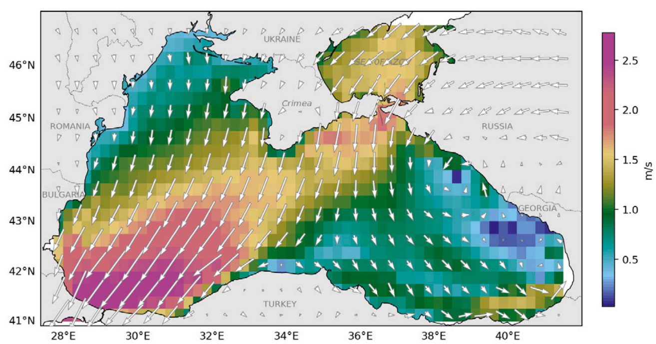

(b) Black Sea mean surface wind speed for the year 2019 (from EU CMEMS-MDS (2024b)).

Fig. 3. Average circulation of ocean currents and surface winds in the Black Sea for the year 2019, used to force particle transport and create Lagrangian trajectories in the PMAR case studies. Note the different scale on the colourbars in the two panels.

coastal retention rate (Miladinova et al., 2020). Each batch of 10000 trajectories (called a "seeding") was created separately and saved as an individual file before aggregation. At the end, 100 seedings were produced ($K = 100$), each starting 3.65 days later than the previous one. This avoids overloading the machine and achieves a total of one million distinct trajectories, which is an order of magnitude generally accepted to give reliable results (Graham and Moyeed, 2002).

Trajectories were calculated using open-source Lagrangian Particle Tracking python package OpenDrift (Dagestad et al., 2018). OpenDrift base module *OceanDrift* was used with a time step of 4 h, a horizontal eddy diffusivity of $10\ \mathrm{m/s^2}$ and a terminal velocity of $0\ \mathrm{m/s}$, to represent the buoyancy of macroplastic litter. Particles were seeded homogeneously over the entire basin, resulting in about 55 particles per cell in the chosen grid for the analysis, with a spatial resolution of $0.05° \times 0.05°$ and a total of 18063 cells. Separate tests showed that increasing the number of particles per cell did not change the result (see Fig. S1).

Particles were advected using ocean and atmospheric model outputs available at the Copernicus Marine Data Store. Northward and eastward velocity of surface ocean currents were extracted from the Copernicus Black Sea physics reanalysis product (EU CMEMS-MDS, 2024a), which provides ocean variables from the year 1993 and is based on general circulation model NEMOv4.0 (Gurvan et al., 2019). The ocean velocities have a horizontal spatial resolution of $0.025° \times 0.025°$ (about 3×3 km) and a daily output. Northward and eastward surface winds were obtained from a global monthly Level-4 product (EU CMEMS-MDS, 2024b) at 0.25° horizontal resolution, based on monthly average ECMWF ERA5 reanalysis fields (Hersbach et al., 2023). No beaching, biofouling, fragmentation or ingestion of macroplastic particles were considered at this stage.

Three main results were produced. First, trajectories were weighted and rasterised as explained in Section 2.3 to obtain the *PPI*. In *NoUse*, since no human activity was identified as the pressure source, a homogeneous map with all cells equal to 1 was used to assign weights (Fig. 4(a)). In *ShippingUse*, weights were extracted from a map of average route density in the Black Sea in 2019 (Fig. 4(b)), which was downloaded from the Human Activities portal on the European Marine Observation and Data Network (EMODNet) Human Activities (2024). The initial condition of *ShippingUse* is shown in Fig. 4(b) and is the same for all seedings. Rasterisation was performed on each seeding, resulting in 100 temporary output files which were then aggregated into a single map to obtain the *PPI* for the year 2019, as defined in Eq. (7). To make the results comparable between *NoUse* and *ShippingUse*, the *PPI* maps are normalised by their total to obtain a percentage.

Next, the boundaries of the Exclusive Economic Zones (EEZ) of Black Sea countries (as defined by Marine Regions, Flanders Marine Institute (2023), see Fig. 4(c)) were used to determine the relative amount of macroplastics ending up in each country (pressure destination), and compare it with the amount released in each country. It is important to note that the initial and final positions of each trajectory are used for this calculation (as opposed to the *PPI*, where trajectories are integrated over time). Finally, the contribution of each country to the amount of macroplastic accumulated in each EEZ was calculated (pressure origin).

2.6. PMAR software implementation

The current version of PMARv0.15 is open-source and developed with Python (v3.9), ensuring high efficiency, flexibility and readability (Wang et al., 2025). It relies on *OpenDrift* ($v \geq 1.14$) (Dagestad et al., 2018), a python package designed to model the trajectories of different objects in the ocean or atmosphere. Through installation of OpenDrift, most package dependencies will be resolved (packages and versions are listed below). In addition, PMAR requires *pandas* ($v \geq 2.2$) (Pandas development team, 2024), *geocube* ($v \geq 0.7$) (Snow et al., 2025), *shapely* ($v \geq 2.1$) (Gillies et al., 2025) and *rioxarray* ($v \geq 0.19$) (Snow et al., 2023) to handle raster data.

The software is built for efficient handling of multidimensional data, relying on *xarray* ($v \geq 2025.4$) (Hoyer et al., 2024) and *pandas* to manage input data, perform analysis of large geospatial datasets, and generate structured outputs. Packages *rioxarray* and *rasterio* ($v \geq 1.4$) (Gillies et al., 2013) facilitate the processing of georeferenced raster data, while *geopandas* ($v \geq 1.0$) (den Bossche et al., 2024) and *shapely* handle vector-based spatial operations.

To improve performance, PMAR employs *dask* ($v \geq 2025.4$) (Dask Development Team, 2016) for parallelised computations, enabling efficient processing of large datasets. It also includes advanced statistical analysis tools, such as histogram-based aggregation with *xhistogram* ($v \geq 0.3$) (Abernathey et al., 2022), and supports high-quality visualisation using *Matplotlib* ($v \geq 3.10$) (Matplotlib Development Team, 2024), *Seaborn* ($v \geq 0.13$) (Waskom, 2021), and *Cartopy* ($v \geq 0.24$) (Elson et al., 2023) for spatial plotting.

A key feature of PMAR is its dynamic access to geospatial and oceanographic data. It connects to the remote interoperable Copernicus Marine Service to retrieve real-time, historical and forecast datasets through OpenDrift Readers, the *copernicusmarine* package ($v \geq 2.0$) (Copernicus Marine Toolbox v2.0.1, 2025), and direct integration with *xarray* for seamless data acquisition and processing.

3. Results

The first software implementation of the PMAR framework is adopted here to investigate pathways of surface macroplastics in the Black Sea, as described in Section 2.5.

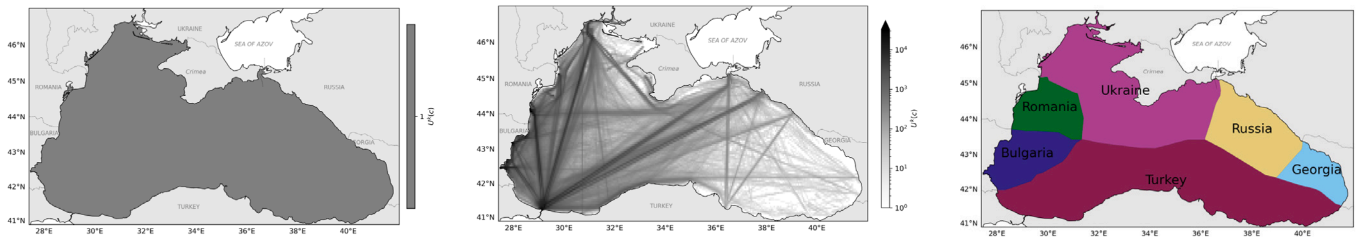

(a) Input raster U for *NoUse*. (b) Input raster U for *ShippingUse*. (c) Boundaries of EEZs.

Fig. 4. Figs. 4(a) and 4(b) show the input rasters $U^k(c)$ used as the pressure source in *NoUse* and *ShippingUse*. Fig. 4(c) shows the boundaries of the Exclusive Economic Zones (EEZs) of Black Sea countries used for further analysis. Colours corresponding to each country are consistent with upcoming figures.

One million distinct trajectories were created and rasterised with two different sets of weights, resulting in two pressure scenarios: *NoUse* and *ShippingUse*. The process of performing 100 seedings to obtain a one year basin-scale simulation, dynamically retrieving data from the Copernicus Marine Data Store on a machine with 16 CPUSs and 30 GB of RAM, took approximately 16 hours for the initial run (during which the trajectory cache was generated) and 15–30 minutes for subsequent runs.

Section 3.1 presents the *PPI* calculated for the two scenarios, while Sections 3.2 and 3.3 analyse the exchanges of macroplastic particles between the different countries within the duration of the run.

3.1. Pressure propagation index (*PPI*) for black sea surface macroplastics

The pressure propagation index (*PPI*) was calculated for each grid cell as in Eq. (7), and then normalised by the sum of all cell weights in both *NoUse* and *ShippingUse*, to obtain a percentage. The *PPI*, shown in Fig. 5, corresponds to the weighted sum of all trajectories passing through each grid cell during the year.

Fig. 5(a) depicts the *PPI* calculated for *NoUse*, where the currents and surface winds are the drivers of particle transport. Indeed, the map mirrors the large scale dynamics of the Black Sea surface circulation (seen in Fig. 3). The anticyclonic rim current pushes floating particles towards the coast of Romania and Turkey on the western side of the basin and away from the coast of Crimea in the north. Mesoscale features are also visible at this resolution; for example, the anticyclonic eddy in the south-eastern region, known as the Batumi eddy, and a filament of high *PPI* exuding from the south-eastern coast.

Compared to the initial condition (Fig. 4(a)), where, in percentage, each cell has a value of 0.005%, the *PPI* is generally lower in the north ($< 0.005\%$) and progressively higher in the south ($\geq 0.005\%$). A downward gradient is formed, with maximum values along the coasts of Bulgaria, Turkey, Georgia and partially Russia (PPI over 0.01%). This is in line with the prevailing northerly winds (Fig. 3(b)), which significantly affect the transport of buoyant objects at the ocean surface by pushing them south.

In *ShippingUse*, shown in Fig. 5(b), the spatial distribution of the *PPI* is affected by the density of shipping routes in the Black Sea, as well as by the general oceanic circulation. The downward gradient appears more pronounced than in *NoUse*, with mostly low *PPI* ($< 0.004\%$) in the northern band from around $44° N$ upwards, with the exception of the Romanian coast. Regions of very high *PPI* (over 0.01%) are concentrated on the western side of the basin, where a higher density of shipping routes is found (as seen in Fig. 4(b)). Overall, this configuration leads to believe that when macroplastic particles are released from ships, coastal areas are more impacted than offshore regions. This is particularly true for the Bosphorus strait, in Turkey, where most of the maritime routes in the Black Sea are directed to.

The *PPI* represented in Fig. 5 can be interpreted as a probability of passage within each cell, as in Van Sebille et al. (2018). This is useful from a management perspective as high *PPI* highlights regions where it is likely to find a concentration of the modelled pressure at any point during the year. An alternative interpretation of the index is that of a snapshot of average yearly concentration, assuming a continuous emission of the pressure from each cell at each time step.

For the sake of this PMAR demonstration, we assumed the release of one macroplastic item per cell in *NoUse* and one per shipping route in *ShippingUse*, i.e. f in Eq. (4) is the identity function, yielding an a-dimensional relative spatial index of pressure intensity within the study area. However, given a known f, this emission may be quantified, providing a realistic picture of mean surface macroplastic concentration in the basin.

3.2. Pressure destination

From a management point of view, it is useful to quantify how much of the pressure being transported in the basin ends up in each country. To make this calculation, the spatial domain was divided into six sub-areas corresponding to the Exclusive Economic Zones (EEZ) of the six Black Sea countries (shown in Fig. 4(c)). The percentage of macroplastics located in each EEZ at the time of their release and at the end of the run is shown in Figs. 6(a) and 6(b), respectively.

The amount of macroplastics per country at the time of release is directly proportional to the surface area of the EEZ in *NoUse* (light grey bars), due to the homogeneous initial condition. As a result, over 40% of the total macroplastics are initially located in Turkey, followed by Ukraine (26%), Russia (12%), Bulgaria and Romania (7%–8%) and Georgia (5%). This distribution differs when trajectories are weighted according to route density (*ShippingUse*): while Turkey still accounts for around 40% of the total macroplastic mass, it is followed here by Bulgaria with almost 30%, then Romania and Ukraine (just under 20%), Russia (1.5%) and Georgia, with only a fraction of the total mass (0.1%).

At the end of the run, most of the released particles end up in Turkey, regardless of their initial condition (Fig. 6(b)). This country collects within its EEZ 70% and 85% of the total macroplastic mass in *NoUse* and *ShippingUse*, respectively. In *NoUse*, this results from a loss of macroplastics in all other countries, with Ukraine and Russia now containing 10% each, and the remaining 10% being distributed across Bulgaria, Romania and Georgia. In *ShippingUse*, the most drastic losses occur in the Western Black Sea countries, particularly Bulgaria and Romania, decreasing to 3% and 1% respectively, and Ukraine, which now only holds 6% of the total macroplastics. Unlike everywhere else, Russia and Georgia end up gathering more particles than they initially held (5% and 2%).

It is important to point out that the indicator shown in Fig. 6 differs from the *PPI*, where trajectories are integrated over time. Here, we are calculating the weighted sum of the trajectories found in each cell at fixed time steps: the time of release and the end of the run. To get the percentage by country, this quantity is then normalised by the total weighted sum of the cells in the grid. Note that the release time differs for each seeding, while the end date of the run is fixed.

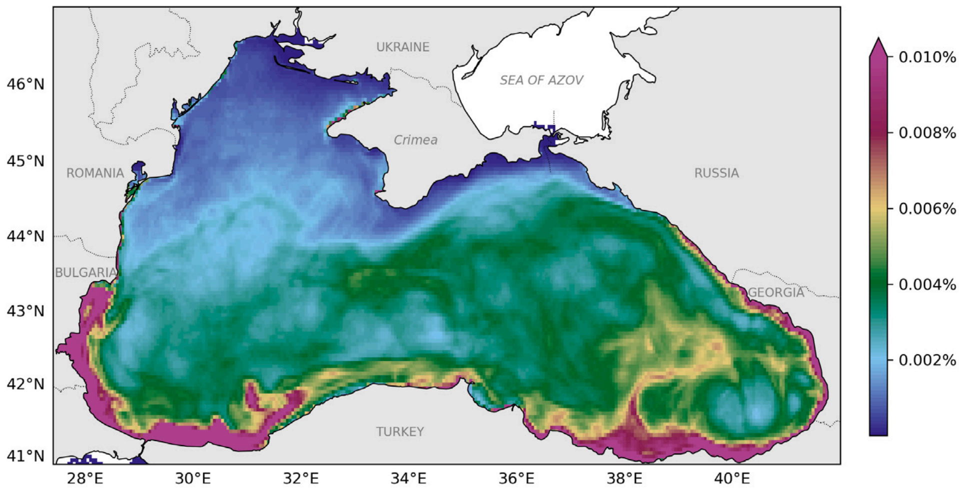

(a) Pressure propagation index (*PPI*) for surface macroplastics in *NoUse*, i.e. with uniform initial condition.

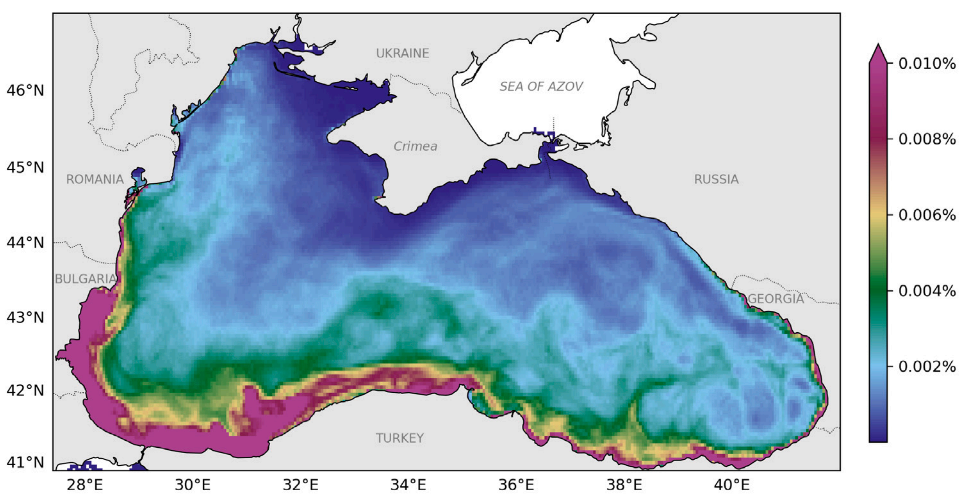

(b) Pressure propagation index (*PPI*) for surface macroplastics in *ShippingUse*, where the initial condition is determined by density of shipping routes.

Fig. 5. Pressure propagation index (*PPI*) resulting from a year-long run, corresponding to the weighted sum of all trajectories passing through each cell over time. The pressure modelled here is surface macroplastics, released from a homogeneous initial condition (*NoUse*, Fig. 5(a)) and from shipping routes (*ShippingUse*, Fig. 5(b)).

The homogeneous seeding of particles partly influences the result shown in Fig. 6 for *NoUse*, since the amount of macroplastics originating from each country depends on the surface area of the corresponding EEZ. The actual emission of macroplastics from each country is not easy to measure. Nevertheless, establishing more realistic relationships between the country and the quantity of pressure it emits during a given time span may be enough to paint an informative picture from an MSP perspective. For example, rather than the surface area covered by the EEZ, the contribution of each country could depend on the size of its coastal cities, or their population, or its rivers. This approach is highly scalable and may be adopted to produce spatial estimates in data-poor conditions.

3.3. Pressure origin

In this section, the contribution of each country to the total amount of macroplastics found in each EEZ at the end of the run (Fig. 6(b)) is calculated. Fig. 7 shows how much of the total mass found in each EEZ at the last time step originated from the other EEZs. This quantity is expressed as a percentage and is shown separately for *NoUse* (Fig. 7(a)) and *ShippingUse* (Fig. 7(b))

In *NoUse*, Turkey and Ukraine appear to be the main contributors of macroplastics, respectively for the eastern and western Black Sea countries. In particular, Turkey accounts for 41,7% of its own macroplastics, making it the country with the highest amount of locally generated pressure. Turkey also accounts for 63% of the particles ending up in Georgia, 57% in Russia and 47% in Ukraine. On the other hand, Ukraine provides the highest contribution to the neighbouring Romania and Bulgaria (over 40%). This configuration is justified by the cyclonic rim current shown in Fig. 3(a) and the large surface areas covered by Ukraine and Turkey.

At least half of the total macroplastics found in each country at the end of the run came from the other EEZs. In particular, from 58.3% (Turkey) up to 92.7% (Bulgaria) of the total macroplastics in each country originated elsewhere, making Bulgaria the country with the highest amount of foreign macroplastics. Portions of the foreign macroplastics found in every EEZ come from each of the other five countries, meaning that all countries collect mass from all others. These

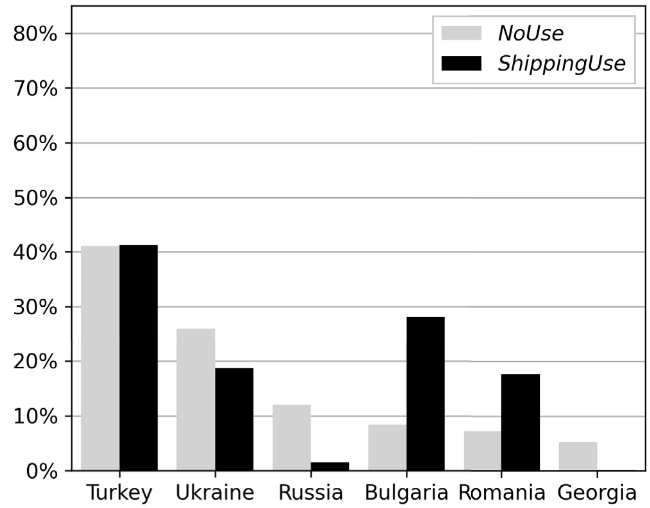

(a) Percentage of macroplastics per country at the time of release for *NoUse* and *ShippingUse*.

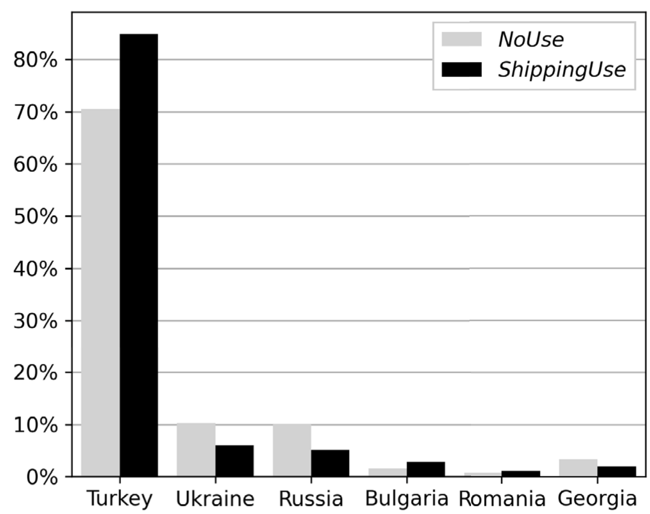

(b) Percentage of macroplastics per country at the end of the run for *NoUse* and *ShippingUse*.

Fig. 6. The amount of macroplastics found in each country's Exclusive Economic Zone (EEZ) at the time of release Fig. 6(a) and at the end of the run Fig. 6(b) is expressed here as a percentage of the total macroplastics in the basin.

results highlight the importance of cross-country collaboration and transnational agreements for the effective management of pressures in dynamic environments such as the Black Sea.

By introducing marine traffic as the source of macroplastics in *ShippingUse* (Fig. 7(b)), the internal exchanges between the different countries are modified. The contributions from Ukraine and Romania increase in the north-western side of the basin, affecting Ukraine, Romania, Bulgaria, while inputs from Georgia and Russia to these countries are nearly zero. In general, local macroplastics increase on this side of the basin compared to *NoUse*. In the south-eastern Black Sea (Turkey, Georgia, Russia), the prevailing origin country remains Turkey, though inputs from Bulgaria are more significant than in *NoUse* for all three countries.

While traffic routes connecting Istanbul (Turkey) to the ports of Odessa (Ukraine), Constanţa (Romania) and Burgas (Bulgaria) increase the fluxes between these four countries, the near-zero contributions from Georgia and Russia may be partly explained by the lack of data on maritime routes on the eastern side of the basin (see Fig. 4(b)). Moreover, the initial conditions influence the final distribution and similar considerations to those in Section 3.2 regarding the correlation between the amount of macroplastic per country and the surface area of their EEZ can be made. In particular, if the general circulation were the only driver of particle transport and all countries released an equal amount of macroplastics, a decrease in the relative contributions from Turkey and Ukraine in favour of the other countries would be expected.

4. Discussion

PMAR is a framework and software aimed at supporting decision-making in marine management through on-demand assessments of anthropogenic pressures at sea originating from different human activities. In the previous section, PMAR was employed to investigate the propagation of surface macroplastics in the Black Sea, as a demonstration of its workflow and capabilities.

The two pressure scenarios, *NoUse* and *ShippingUse*, highlighted a southward gradient of *PPI*, with highest values in the Southern coast of the Black Sea. This is in line with the general anticyclonic circulation in the basin and prevailing westerlies which cause upwelling in the interior (Stanev and Ricker, 2019). No long-term offshore accumulation is identified, as expected at the spatial and temporal scales of Black Sea circulation (Miladinova et al., 2020). Turkey and Ukraine emerge as the largest contributors to the macroplastic accumulation of all Black Sea countries, as revealed by previous studies (González-Fernández et al., 2021).

In the coming sections, we focus on validating the model by first comparing results of the case study with observational data from visual surveys carried out in the Black Sea between 2017 and 2019 (Section 4.1). Next, we set up a toy problem to be reproduced with two other existing open-source modelling frameworks that are suitable for pressure assessment, Tools4MSP (Menegon et al., 2018c) and OpenDrift (Dagestad et al., 2018), and compare with PMAR results (Section 4.2). Finally, we discuss the limitations of the current version of PMAR and anticipate planned improvements for future work (Section 4.3).

4.1. Comparison with in situ observations

No long-term and high-coverage monitoring study of floating marine macroplastic in the Black Sea is currently published. Measurements from existing monitoring efforts are primarily coastal (Özşeker et al., 2024; Bekova and Prodanov, 2024; Berov and Klayn, 2020; Simeonova and Chuturkova, 2020; Topçu et al., 2013), making it difficult to compare with our basin-wide case study.

Nevertheless, González-Fernández et al. (2022) performed a series of surveys based on visual observations, crossing the basin from North to South and from West to East, for a total of 302 monitoring sessions that took place from May to November 2017 and from June to October 2019. They calculated the abundance of macroplastics in four distinct geographical regions in the Black Sea: Western offshore (W-OS), Eastern offshore (E-OS), Western Territorial Sea (W-TS) and Eastern Territorial Sea (E-TS).

The transects by González-Fernández et al. (2022), which cover the Black Sea interior, provide an opportunity for comparison with our basin-wide modelled result. It should be noted, however, that this type of monitoring data can be affected by seasonal and interannual variability, by weather conditions during field work, and by the individual ability of the surveyors to spot and recognise plastic items at a distance. In addition, we are here comparing point-wise observations with an average basin-wide model result (the *PPI*). We therefore do not expect full numerical agreement between the two but, rather, are

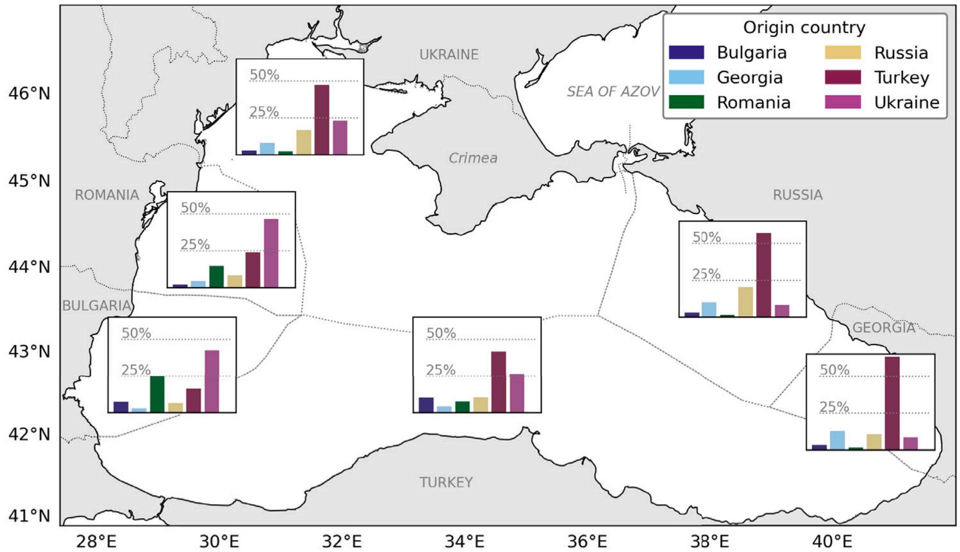

(a) Homogeneous initial condition (*NoUse*).

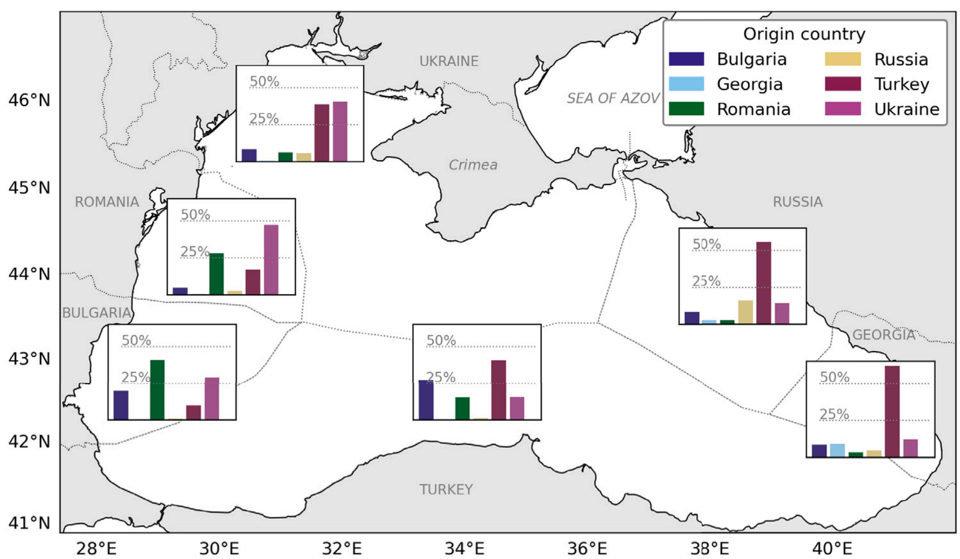

(b) Macroplastics released from shipping (*ShippingUse*).

Fig. 7. Origin attribution of macroplastics across Black Sea Exclusive Economic Zones (EEZ). The bar plots show, for each EEZ, the fraction of the macroplastics present at the end of the simulation that originated from the EEZs of the six Black Sea countries. Fig. 7(a) refers to *NoUse*, while Fig. 7(b) refers to *ShippingUse*.

looking for consistency in the relative distribution between the four regions.

Since no information is provided as to the potential sources of the macroplastic items surveyed in González-Fernández et al. (2022), we compare the total number of items found in each region, in percentage, with the total *NoUse PPI* in the corresponding region. The result is shown in Fig. S2.

Overall, the *PPI* agrees with the observational data provided by González-Fernández et al. (2022) in the relative distribution between the four areas, with the majority of items found in E-OS, followed by W-OS, then E-TS and W-TS. In general, a higher accumulation appears offshore rather than in territorial waters, and in the eastern rather than the western basin. This discrepancy is more dramatic in the observational data than in PMAR, where nearly 65% of all items were detected in the E-OS region (41% in PMAR *NoUse*).

4.2. Comparison with existing models

To further validate PMAR results, two python-based, free, open-source software frameworks are employed to reproduce a PMAR toy problem simulating the dispersal of macroplastics from shipping routes: Tools4MSP and OpenDrift.

Tools4MSP is a framework for geospatial analysis in support of Maritime Spatial Planning (MSP) (Menegon et al., 2018c). By default, it simulates pressure propagation from a given source by implementing an isotropic distance-based model with a Gaussian kernel function applied to the source raster (for more details, see Menegon et al. (2018a)). As Tools4MSP does not rely on ocean dynamics to simulate pressure propagation, we expect significant differences in the spatial distribution of macroplastics compared to PMAR.

OpenDrift is a highly generic and modular software framework for Lagrangian particle modelling, designed for any type of drift calculations in the ocean or atmosphere (Dagestad et al., 2018). As explained above, PMAR employs OpenDrift to create trajectories, which are then rasterized and aggregated to produce the *PPI*. However, by using OpenDrift natively, we do not have the option to connect the pressure and its source through trajectory weights. Therefore, we expect similar, but not identical, results compared to PMAR.

The toy problem is a simplified version of *ShippingUse*, discussed above. The propagation of surface macroplastics from maritime traffic routes is simulated in the south-western Black Sea, around the Bosporus strait. Particles are seeded within a bounding box defined by the following limits: longitude = $[27.5^\circ E, 32^\circ E]$, latitude = $[41^\circ N, 43^\circ N]$. The run starts on the 1st of January 2019 and particle positions are recorded every hour for 30 days. Particles are advected using current and wind velocity fields described in Section 2.5. The raster taken as the pressure source is a map of yearly route density (2019, European Marine Observation and Data Network (EMODNet) Human Activities (2024)), which is rescaled to match the duration of the run. A two-dimensional grid of $0.05^\circ \times 0.05^\circ$ resolution is used to produce the maps, which are then normalised by their total to obtain a percentage for easier comparison.

In PMAR, particles are seeded homogeneously within the bounding box (see Fig. S3). Weights are extracted from the source raster, assigned to trajectories, and the *PPI* is calculated as described in Section 2.3.

To obtain a comparable result using OpenDrift natively, i.e. in the absence of PMAR's weight-based mechanism, we seeded a number of particles in each $0.05^\circ \times 0.05^\circ$ grid cell that is directly proportional to the value of the route density raster, for a total of 19224 particles (see Fig. S3, the same amount of particles is seeded in the PMAR case). We then calculate a two-dimensional histogram using OpenDrift's native method `get_histogram` with a `pixel_size` of 5 km, to roughly match the $0.05^\circ \times 0.05^\circ$ resolution of the reference grid.

Finally, to obtain an analogous result with Tools4MSP, the map of monthly route density is fed to the model, which applies the Gaussian kernel function and returns a map of macroplastics released from traffic routes on the reference grid.

The Tools4MSP approach shows almost no dispersal outside of the initial bounding box (black square in Fig. S4). However, according to the two trajectory-based approaches, PMAR and OpenDrift, significant propagation does occur outside of this perimeter in a 30-day run (Fig. S4). In addition, the Gaussian kernel used in Tools4MSP results in a circular hotspot at the Bosphorus entrance (where traffic is highest), while the inclusion of ocean and atmospheric dynamics in PMAR and OpenDrift produces a more complex shape in the same region of high concentration.

To better compare the three outputs, we calculate the spatial (pixel by pixel) difference between Tools4MSP and PMAR with Opendrift (see Fig. 8). OpenDrift is taken as the reference result since the tool has been adopted in a variety of peer-reviewed scientific publications, both by its creators (Dagestad et al., 2018; Aghito et al., 2023) and by international researchers (Mohrmann et al., 2025; Nadal et al., 2024) and is currently in use within services from MET Norway, Chilean Fisheries Service (IFOP) and the Irish Marine Institution (Services using OpenDrift, 2025). The zonal and meridional concentrations resulting from the three models are also shown in the line plots, to highlight similarities.

A clear spatial difference is visible between Tools4MSP and OpenDrift: Tools4MSP overestimates the amount of pressure on the western side, while it underestimates the amount close to the Turkish coast travelling eastward (Fig. 8(a)).

On the other hand, the difference between PMAR and OpenDrift does not show a clear spatial pattern and has on average lower values (Fig. 8(b)). Despite a different seeding pattern at the initial condition (homogeneous in PMAR and proportional to the shipping routes in OpenDrift, as shown in Fig. S3), the two results are in agreement, suggesting that the weight-based method adopted in PMAR provides a valid alternative to simply seeding more particles where more shipping routes are located.

Assigning weights to pre-calculated trajectories to simulate different pressure sources provides various advantages. First, since the proportionality between the source and the pressure is given by a value associated to the trajectories in a cell (the weight), and not by the number of trajectories seeded in a cell, we avoid creating huge datasets with extremely high numbers of trajectories. Second, by applying weights on pre-calculated trajectories we are able to quickly test different scenarios of pressure propagation. In this toy problem, the calculation of trajectories took 10 minutes in both PMAR and OpenDrift, while the creation of the map took 10 seconds. This means that each new pressure source scenario would take 10 min if using OpenDrift natively (since simulating a new set of trajectories would be required), and only 10 s if using PMAR (since it would only entail assigning new weights and recalculating the *PPI* map), with comparable results.

4.3. Model limitations and future work

We assume that the data driving particle transport in PMAR is close to the best available, as we used widely adopted and validated velocity fields from Copernicus. In addition, we seeded a high number of particles (compared to e.g. Stanev and Ricker, 2019), which increases accuracy (Van Sebille et al., 2018; Graham and Moyeed, 2002). Nevertheless, like all modelling approaches, PMAR has limitations due to underlying assumptions and to the expeditious nature of this type of "on-demand" analysis.

Firstly, Lagrangian trajectories are suited for modelling tracers carried by seawater (Van Sebille et al., 2018). This includes about 50% of anthropogenic pressures identified by the MSFD, such as the introduction or spread of non-indigenous species, nutrients, organic matter, litter, water, radionuclides and other synthetic and non-synthetic substances. Other types of modelling tools would be better suited for the remaining pressures, e.g., underwater noise or other forms of energy whose dispersion is governed by different physics than matter (Ghezzo et al., 2024), physical pressures (e.g. disturbance or loss of seabed), and some biological pressures (e.g. the extraction, mortality or injury of species). While half of MSFD-defined pressures can be modelled with the current configuration, it is our aspiration that PMAR should include a suite of appropriate modelling tools to eventually cover the majority of them.

Another limitation lies in the need to perform the initial calculation of the desired set of trajectories in the area of analysis. This preliminary computation can be lengthy, especially if looking at a large geographical region (scale of a full basin) and if seeding a high number of particles, which is required to obtain a statistically significant result (Graham and Moyeed, 2002). However, this "loss" of computational time is compensated by the possibility to estimate different pressure source scenarios almost in real-time (order of seconds) thanks to the weight-based mechanism.

Next, the case study on surface macroplastics in the Black Sea was simplified as much as possible, overlooking some physical features which may have otherwise influenced the result. We assumed that macroplastic particles were highly buoyant and would therefore not experience sinking at the timescales here considered. We did not account for potential fragmentation, biofouling, or beaching of particles. The velocity fields used to calculate trajectories did not include the Stokes drift, under the assumption that it would be similar to the wind field (Stanev and Ricker, 2019), despite this feature being recommended when modelling buoyant objects at the sea surface (van den Bremer and Breivik, 2018; Bosi et al., 2021). The above choices were made as the focus of this paper was the methodology of the PMAR framework, rather than the case study. Nevertheless, PMAR is fully equipped to account for those physical aspects, thanks to the choice of python packages it relies on (e.g. OpenDrift).

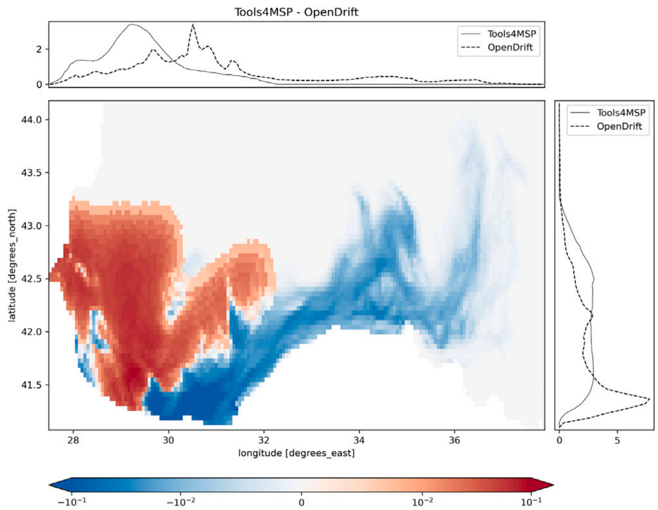

(a) Spatial difference between the Tools4MSP result of the toy problem, and the OpenDrift result.

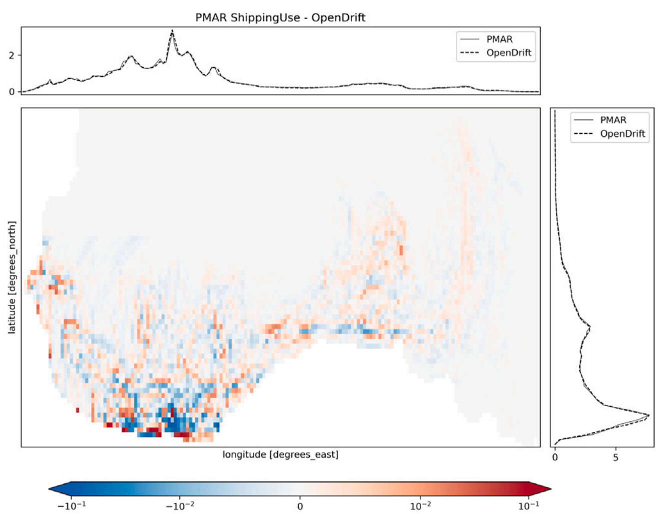

(b) Spatial difference between the PMAR result of the toy problem, and the OpenDrift result.

Fig. 8. Spatial difference of the toy problem results. OpenDrift is taken as reference and subtracted pixel by pixel from Tools4MSP 8(a) and PMAR 8(b). Note the logarithmic scale in the colour bar. The line plots show the zonal and meridional distribution of the *PPI* or macroplastics concentration for the respective models.

Future improvements will focus on further aligning PMAR with the requirements of Digital Twin of the Ocean (DTO) applications for MSP, such as the ability to perform real-time analysis to respond to different management questions (Bosi et al., 2025). While the current weighted trajectory set-up allows for quick computation of different scenarios, we plan on adopting connectivity matrices to make predictions of pressure concentration both forwards and backwards in time. Connectivity matrices provide insight on the exchanges of material between different regions (Liu et al., 2025) and thus support the analysis of future scenarios, which is increasingly recognised as a key step of the MSP process (Calado et al., 2021).

Further efforts will aim at making the tool accessible to non-technical users (e.g. decision-makers). The current pipeline developed within PMAR allows users to perform the calculation of trajectories and related maps of pressure propagation simply by inputting a handful of parameters and launching a single function. However, this process still requires some python knowledge. The final goal is to develop an intuitive Graphical User Interface to make PMAR fully accessible as a Decision Support Tool (DST). Recent reflections on the use of Design Thinking in the context of Maritime Spatial Planning (Zancanaro et al., 2025) highlight how participatory and iterative design processes can help align digital tools with the needs and workflows of end users. Building on this perspective, adopting Design Thinking principles could support the continuous improvement of PMAR towards a more user-centred and accessible design.

Finally, a systematic Sensitivity and Uncertainty Analysis (SUA) should be carried out to identify parameters whose variations most affect PMAR results (Zhong et al., 2024). Results of a SUA would also serve as a guide for potential users in configuring the tool and correctly interpreting PMAR outputs.

5. Conclusion

In this paper we presented PMAR (Pressure models for MARine activities), a framework and software for the modelling and assessment of anthropogenic pressures at sea designed for marine management. We investigated the propagation of surface macroplastics in the Black Sea using PMAR software v0.15. We produced maps of a Pressure Propagation Index (*PPI*), representing the dispersal of macroplastics from different sources (*NoUse* and *ShippingUse* scenarios). We then explored how macroplastics released in the Exclusive Economic Zones (EEZs) of the different Black Sea countries were redistributed in the other countries over the year. Finally, we compared PMAR results with data from *in situ* observations in the Black Sea and with other existing frameworks for pressure modelling, and we concluded by identifying limitations of the tool and opportunities for future work.

PMAR proved effective in modelling surface macroplastics by yielding comparable results to other modelling studies in the area, as well as *in situ* surveys. The analysis on the origin and destination of macroplastics emphasised how PMAR results can support marine management by identifying which countries are the most significant sources (Turkey, Ukraine) and sinks (Bulgaria). Importantly, we found that all countries collect macroplastics in their EEZ from all other countries in the basin. In particular, at least half of the macroplastics accumulated within a Black Sea country's EEZ came from elsewhere, stressing the importance of transboundary cooperation in marine management.

The comparison with other modelling frameworks (Tools4MSP and OpenDrift) identified PMAR as a convincing trade-off between efficiency and accuracy in pressure modelling, yielding fast computation of pressure scenarios and realistic results. Through the Pressure Propagation Index (*PPI*), PMAR provides an explicit linkage between anthropogenic uses, pressure sources, and their spatial distribution, thus contributing to the improvement of traditional Cumulative Effects Assessment (CEA) methods. This aligns with the need for data contextualisation within CEA for MSP, ensuring that modelling results are not only spatially explicit, but also functional for planners and stakeholders, facilitating evidence-based decision-making.

PMAR establishes a standardised framework for assessing different types of pressures in combination with existing CEA methodologies. The framework is highly scalable and can be applied to different spatial and temporal domains, scales, anthropogenic pressures and management questions. Fully designed from an MSP perspective, it responds to specific MSPD articles, namely: Art. 4, requiring marine planners and decision-makers to consider impacts of human activities on the marine environment; Art. 5, for the adoption of an Ecosystem-Based Approach; Art. 10, calling for the use of the best available data; and Art. 11, which stresses the importance of transboundary effects.

Although the current implementation entirely relies on Lagrangian modelling, we plan to incorporate alternative pressure dispersion mechanisms, such as chemical dispersion models agent-based models for biological stressors (e.g., invasive species), or acoustic propagation models for noise pollution.

While PMAR is designed as a standalone tool, it can also be seamlessly incorporated into the Tools4MSP CEA module, supporting CEA-Lagrangian dispersion coupling. This integration enhances its applicability within existing MSP workflows, ensuring compatibility with established methodologies. In addition, the "light-weight" nature of the tool and its ability to produce on-demand scenarios aligns with emerging Digital Twins of the Ocean (DTO).

CRediT authorship contribution statement

Sofia Bosi: Writing – review & editing, Writing – original draft, Visualization, Software, Methodology, Investigation, Formal analysis, Data curation, Conceptualization. **Alessandra Raffaetà:** Writing – review & editing, Writing – original draft, Supervision, Methodology. **Marta Simeoni:** Writing – review & editing, Supervision, Methodology. **Nikola Bobchev:** Writing – review & editing, Writing – original draft. **Dimitar Berov:** Writing – review & editing, Writing – original draft. **Andrea Barbanti:** Writing – review & editing, Funding acquisition. **Stefano Menegon:** Writing – review & editing, Writing – original draft, Supervision, Methodology, Investigation, Conceptualization.

Declaration of competing interest

The authors declare the following financial interests/personal relationships which may be considered as potential competing interests: Sofia Bosi reports financial support was provided by European Union. If there are other authors, they declare that they have no known competing financial interests or personal relationships that could have appeared to influence the work reported in this paper.

Acknowledgements

This work was financed by the project BRIDGE-BS (Advancing Black Sea Research and Innovation to Co-Develop Blue Growth within Resilient Ecosystems), funded by the European Union's Horizon 2020 research and innovation programme under grant agreement ID 101000240. This work also took place within the framework of the DoE 2023–2027 (MUR, AIS.DIP.ECCELLENZA2023_27.FF project).

Appendix A. Supplementary data

Supplementary material related to this article can be found online at https://doi.org/10.1016/j.envsoft.2025.106822.

Data availability

Data supporting the findings of this study were derived from the following resources available in the public domain: EU CMEMS-MDS (2024a), EU CMEMS-MDS (2024b) and European Marine Observation and Data Network (EMODNet) Human Activities (2024).

References

Abernathey, R., Squire, D., Nicholas, T., Bourbeau, J., Joseph, G., Spring, A., Bell, R., Bailey, S., 2022. xhistogram. Zenodo, http://dx.doi.org/10.5281/zenodo.7095156.

Aghito, M., Calgaro, L., Dagestad, K.-F., Ferrarin, C., Marcomini, A., Breivik, Ø., Hole, L.R., 2023. ChemicalDrift 1.0: an open-source Lagrangian chemical-fate and transport model for organic aquatic pollutants. Geosci. Model. Dev. 16 (9), 2477–2494. http://dx.doi.org/10.5194/gmd-16-2477-2023.

Andrady, A.L., 2015. Persistence of plastic litter in the oceans. In: Bergmann, M., Gutow, L., Klages, M. (Eds.), Marine Anthropogenic Litter. Springer International Publishing, Cham, pp. 57–72. http://dx.doi.org/10.1007/978-3-319-16510-3_3.

Baharvand, S., Ahmari, H., Taghvaei, P., 2023. Developing a Lagrangian sediment transport model for open channel flows. Int. J. Sediment Res. 38 (2), 153–165.

Bekova, R., Prodanov, B., 2024. Spatiotemporal variation in marine litter distribution along the Bulgarian black sea sandy beaches: amount, composition, plastic pollution, and cleanliness evaluation. Front. Mar. Sci. 11, 1416134. http://dx.doi.org/10.3389/fmars.2024.1416134.

Berov, D., Klayn, S., 2020. Microplastics and floating litter pollution in Bulgarian black sea coastal waters. Marine Poll. Bull. 156, 111225. http://dx.doi.org/10.1016/j.marpolbul.2020.111225.

Bobchev, N., Berov, D., Klayn, S., Karamfilov, V., 2024. High microplastic pollution in marine sediments associated with urbanised areas along the SW Bulgarian black sea coast. Marine Poll. Bull. 209, 117150. http://dx.doi.org/10.1016/j.marpolbul.2024.117150.

Bosi, S., Barbanti, A., Fadini, A., Gissi, E., Mulazzani, A., Ramieri, E., Sarretta, A., Menegon, S., 2025. Leveraging Digital Twins of the Ocean for Integrated and Participatory Approaches for Sustainable Ocean Management. In: One Ocean Science Congress 2025, Nice, France, 3–6 Jun 2025, OOS2025-1325. http://dx.doi.org/10.5194/oos2025-1325.

Bosi, S., Broström, G., Roquet, F., 2021. The role of Stokes drift in the dispersal of north Atlantic surface marine debris. Front. Mar. Sci. 8, 697430. http://dx.doi.org/10.3389/fmars.2021.697430.

Bosi, S., Ramieri, E., Picciulin, M., Menegon, S., Ghezzo, M., Petrizzo, A., Folegot, T., Madricardo, F., Barbanti, A., 2023. Is maritime spatial planning a tool to mitigate the impacts of underwater noise? A review of adopted and upcoming maritime spatial plans in Europe. Mar. Policy 155, 105725. http://dx.doi.org/10.1016/j.marpol.2023.105725.

BSC, 2007. Marine Litter in the Black Sea Region: A Review of the Problem. Black Sea Commission Publications 2007-1, Istanbul, Turkey, p. 160.

BSC, 2019. In: Krutov, A. (Ed.), State of the Environment of the Black Sea. Publications of the Commission on the Protection of the Black Sea Against Pollution (BSC) 2009-2014/5, Istanbul, Turkey, p. 811.

Calado, H., Pegorelli, C., Vergílio, M., Hipólito, C., Campos, A., Moniz, F., Costa, A.C., da Silva, C.P., Fonseca, C., Santos, C.F., et al., 2021. Expert knowledge-based co-development of scenarios for maritime spatial planning in the northeast Atlantic. Mar. Policy 133, 104741.

Copernicus Marine Toolbox v2.0.1, 2025. URL https://github.com/mercator-ocean/copernicus-marine-toolbox. (Accessed November 2025).

Council of the European Union, European Parliament, 2008. Directive 2008/56/EC of the European parliament and of the council of 17 june 2008 establishing a framework for community action in the field of marine environmental policy (marine strategy framework directive. URL https://eur-lex.europa.eu/eli/dir/2008/56/oj/eng.

Council of the European Union, European Parliament, 2014. Directive 2014/89/EU of the European parliament and of the council of 23 july 2014 establishing a framework for maritime spatial planning. URL http://data.europa.eu/eli/dir/2014/89/oj.

Dagestad, K.-F., Röhrs, J., Breivik, Ø., Ådlandsvik, B., 2018. OpenDrift v1. 0: a generic framework for trajectory modelling. Geosci. Model. Dev. 11, 1405–1420. http://dx.doi.org/10.5194/gmd-11-1405-2018.

Dask Development Team, 2016. Dask: Library for dynamic task scheduling. URL http://dask.pydata.org.

den Bossche, J.V., Jordahl, K., Fleischmann, M., McBride, J., Richards, M., Wasserman, J., Badaracco, A.G., Snow, A.D., Ward, B., Gerard, J., Tratner, J., Perry, M., Farmer, C., Hjelle, G.A., Taves, M., ter Hoeven, E., Cochran, M., Rraymondgh, Bartos, M., Bell, R., Culbertson, L., Caria, G., Eubank, N., Roggemans, P., Sangarshanan, Flavin, J., Rey, S., Gardiner, J., Kaushik, 2024. geopandas/geopandas: v0.14.3. Zenodo, http://dx.doi.org/10.5281/zenodo.10601680.

Depellegrin, D., Hansen, H.S., Schrøder, L., Bergström, L., Romagnoni, G., Steenbeek, J., Gonçalves, M., Carneiro, G., Hammar, L., Pålsson, J., et al., 2021. Current status, advancements and development needs of geospatial decision support tools for marine spatial planning in European seas. Ocean & Coastal Management 209, 105644. http://dx.doi.org/10.1016/j.ocecoaman.2021.105644.

Elliott, M., Borja, A., Cormier, R., 2020. Activity-footprints, pressures-footprints and effects-footprints–walking the pathway to determining and managing human impacts in the sea. Marine Poll. Bull. 155, 111201. http://dx.doi.org/10.1016/j.marpolbul.2020.111201.

Elson, P., de Andrade, E.S., Lucas, G., May, R., Hattersley, R., Campbell, E., Dawson, A., Little, B., Raynaud, S., Scmc72, Snow, A.D., Comer, R., Donkers, K., Blay, B., Killick, P., Wilson, N., Peglar, P., Lgolston, Lbdreyer, Andrew, Szymaniak, J., Berchet, A., Bosley, C., Davis, L., Filipe, Krasting, J., Bradbury, M., Kirkham, D., Stephenworsley, Havlin, C., 2023. SciTools/cartopy: v0.22.0. Zenodo, http://dx.doi.org/10.5281/zenodo.8216315.

EU CMEMS-MDS, 2024a. Copernicus marine service information (CMEMS). Marine data store (MDS). Black sea physics reanalysis. http://dx.doi.org/10.48670/mds-00356.

EU CMEMS-MDS, 2024b. Copernicus marine service information (CMEMS). Marine data store (MDS). Global ocean monthly mean sea surface wind and stress from scatterometer and model. http://dx.doi.org/10.48670/moi-00181.

European Marine Observation and Data Network (EMODNet) Human Activities, 2024. EMODnet_HA_EMSA_Route_Density_Map_20191111. URL https://emodnet.ec.europa.eu/en/human-activities. (Accessed April 2025).

European Ocean Pact stakeholder group, 2024. Manifesto for a European Ocean Pact. Oceano Azul Foundation, Europe Jacques Delors, URL https://www.europejacquesdelors.eu/publications/manifesto-for-a-european-ocean-pact.

Farella, G., Menegon, S., Fadini, A., Depellegrin, D., Manea, E., Perini, L., Barbanti, A., 2020. Incorporating ecosystem services conservation into a scenario-based MSP framework: An adriatic case study. Ocean & Coastal Management 193, 105230. http://dx.doi.org/10.1016/j.ocecoaman.2020.105230.

Farella, G., Tassetti, A.N., Menegon, S., Bocci, M., Ferrà, C., Grati, F., Fadini, A., Giovanardi, O., Fabi, G., Raicevich, S., Barbanti, A., 2021. Ecosystem-based MSP for enhanced Fisheries sustainability: An example from the northern Adriatic (Chioggia—Venice and Rovigo, Italy). Sustainability 13 (3), 1211. http://dx.doi.org/10.3390/su13031211.

Fernandes, M.d.L., Esteves, T.C., Oliveira, E.R., Alves, F.L., 2017. How does the cumulative impacts approach support maritime spatial planning? Ecol. Indic. 73, 189–202. http://dx.doi.org/10.1016/j.ecolind.2016.09.014.

Flanders Marine Institute, 2023. Maritime boundaries geodatabase, version 12. http://dx.doi.org/10.14284/628, URL https://www.marineregions.org/.

Ghezzo, M., Petrizzo, A., Madricardo, F., Folegot, T., Gallou, R., Clorennec, D., Chavanne, R., Hemon, E., Ferrarin, C., Mihanović, H., et al., 2024. Natural and shipping underwater sound distribution in the northern Adriatic sea basin and possible application on target areas. Marine Poll. Bull. 207, 116852.

Gillies, S., van der Wel, C., Van den Bossche, J., Taves, M.W., Arnott, J., Ward, B.C., et al., 2025. Shapely. Zenodo, http://dx.doi.org/10.5281/zenodo.15130011.

Gillies, S., et al., 2013. Rasterio: Geospatial Raster I/O for Python Programmers. Mapbox, URL https://github.com/rasterio/rasterio.

Gissi, E., Menegon, S., Sarretta, A., Appiotti, F., Maragno, D., Vianello, A., Depellegrin, D., Venier, C., Barbanti, A., 2017. Addressing uncertainty in modelling cumulative impacts within maritime spatial planning in the Adriatic and ionian region. In: Hewitt, J. (Ed.), PLOS ONE 12 (7), http://dx.doi.org/10.1371/journal.pone.0180501.

Goeury, C., Hervouet, J.-M., Baudin-Bizien, I., Thouvenel, F., 2014. A Lagrangian/Eulerian oil spill model for continental waters. J. Hydraul. Res. 52 (1), 36–48. http://dx.doi.org/10.1080/00221686.2013.841778.

González-Fernández, D., Cózar, A., Hanke, G., Viejo, J., Morales-Caselles, C., Bakiu, R., Barceló, D., Bessa, F., Bruge, A., Cabrera, M., et al., 2021. Floating macrolitter leaked from Europe into the ocean. Nat. Sustain. 4 (6), 474–483. http://dx.doi.org/10.1038/s41893-021-00722-6.

González-Fernández, D., Hanke, G., Pogojeva, M., Machitadze, N., Kotelnikova, Y., Tretiak, I., Savenko, O., Bilashvili, K., Gelashvili, N., Fedorov, A., et al., 2022. Floating marine macro litter in the black sea: Toward baselines for large scale assessment. Environ. Pollut. 309, 119816. http://dx.doi.org/10.1016/j.envpol.2022.119816.

Graham, D.I., Moyeed, R.A., 2002. How many particles for my Lagrangian simulations? Powder Technol. 125 (2–3), 179–186.

Gurvan, M., Bourdallé-Badie, R., Chanut, J., Clementi, E., Coward, A., Ethé, C., Iovino, D., Lea, D., Lévy, C., Lovato, T., Martin, N., Masson, S., Mocavero, S., Rousset, C., Storkey, D., Vancoppenolle, M., Müeller, S., Nurser, G., Bell, M., Samson, G., 2019. NEMO Ocean Engine. Zenodo, http://dx.doi.org/10.5281/zenodo.3878122.

Halpern, B.S., Kappel, C.V., Selkoe, K.A., Micheli, F., Ebert, C.M., Kontgis, C., Crain, C.M., Martone, R.G., Shearer, C., Teck, S.J., 2009. Mapping cumulative human impacts to California current marine ecosystems. Conserv. Lett. 2 (3), 138–148. http://dx.doi.org/10.1111/j.1755-263X.2009.00058.x.

Halpern, B.S., Walbridge, S., Selkoe, K.A., Kappel, C.V., Micheli, F., d'Agrosa, C., Bruno, J.F., Casey, K.S., Ebert, C., Fox, H.E., et al., 2008. A global map of human impact on marine ecosystems. Science 319 (5865), 948–952. http://dx.doi.org/10.1126/science.1149345.

Hammar, L., Molander, S., Pålsson, J., Crona, J.S., Carneiro, G., Johansson, T., Hume, D., Kågesten, G., Mattsson, D., Törnqvist, O., et al., 2020. Cumulative impact assessment for ecosystem-based marine spatial planning. Sci. Total Environ. 734, 139024. http://dx.doi.org/10.1016/j.scitotenv.2020.139024.

Hansen, H.S., 2019. Cumulative impact of societal activities on marine ecosystems and their services. In: Computational Science and Its Applications – ICCSA 2019. Springer International Publishing, Cham, pp. 577–590. http://dx.doi.org/10.1007/978-3-030-24302-9_41.

Heinänen, S., Mannerla, M., Vinther, M., 2013. Human uses, pressures and impacts in the eastern north sea. In: Andersen, J., Stock, A. (Eds.), In: Technical Report from DCE – Danish Centre for Environment and Energy, (no. 18), Aarhus University, DCE - Danish Centre for Environment and Energy, URL http://www.dmu.dk/Pub/TR18.pdf.

HELCOM, 2019. Spatial pressures and impact assessment (SPIA). URL https://github.com/helcomsecretariat/Cumulative-impact-Assessment-Toolbox.

HELCOM, 2023. Thematic assessment of spatial distribution of pressures and impacts 2016–2021. Baltic sea environment proceedings. no. 189. URL https://helcom.fi/wp-content/uploads/2023/03/HELCOM-Thematic-assessment-of-spatial-distribution-of-pressures-and-impacts-2016-2021.pdf.

Hersbach, H., Bell, B., Berrisford, P., Biavati, G., Horányi, A., Muñoz Sabater, J., Nicolas, J., Peubey, C., Radu, R., Rozum, I., et al., 2023. ERA5 hourly data on single levels from 1940 to present, Copernicus Climate Change Service (C3S) Climate Data Store (CDS)[data set].

Hoyer, S., Roos, M., Joseph, H., Magin, J., Cherian, D., Fitzgerald, C., Hauser, M., Fujii, K., Maussion, F., Imperiale, G., Clark, S., Kleeman, A., Nicholas, T., Kluyver, T., Westling, J., Munroe, J., Amici, A., Barghini, A., Banihirwe, A., Bell, R., Hatfield-Dodds, Z., Abernathey, R., Bovy, B., Omotani, J., Mühlbauer, K., Roszko, M.K., Wolfram, P.J., 2024. xarray. Zenodo, http://dx.doi.org/10.5281/zenodo.10676856.

Jones, F.C., 2016. Cumulative effects assessment: theoretical underpinnings and big problems. Environ. Rev. 24 (2), 187–204. http://dx.doi.org/10.1139/er-2015-0073.

Judd, A., Backhaus, T., Goodsir, F., 2015. An effective set of principles for practical implementation of marine cumulative effects assessment. Environ. Sci. Policy 54, 254–262. http://dx.doi.org/10.1016/j.envsci.2015.07.008.

Kale, G., Kijchavengkul, T., Auras, R., Rubino, M., Selke, S.E., Singh, S.P., 2007. Compostability of bioplastic packaging materials: an overview. Macromol. Biosci. 7 (3), 255–277. http://dx.doi.org/10.1002/mabi.200600168.

Korpinen, S., Meski, L., Andersen, J.H., Laamanen, M., 2012. Human pressures and their potential impact on the Baltic sea ecosystem. Ecol. Indic. 15 (1), 105–114. http://dx.doi.org/10.1016/j.ecolind.2011.09.023.

Kotta, J., Fetissov, M., Szava-Kovats, R., Aps, R., Martin, G., 2020. Online tool to integrate evidence-based knowledge into cumulative effects assessments: Linking human pressures to multiple nature assets. Environ. Adv. 2, 100026. http://dx.doi.org/10.1016/j.envadv.2020.100026.

Lebreton, L., Slat, B., Ferrari, F., Sainte-Rose, B., Aitken, J., Marthouse, R., Hajbane, S., Cunsolo, S., Schwarz, A., Levivier, A., et al., 2018. Evidence that the Great Pacific Garbage Patch is rapidly accumulating plastic. Sci. Rep. 8 (1), 4666.

Lechner, A., Keckeis, H., Lumesberger-Loisl, F., Zens, B., Krusch, R., Tritthart, M., Glas, M., Schludermann, E., 2014. The Danube so colourful: a potpourri of plastic litter outnumbers fish larvae in Europe's second largest river. Environ. Pollut. 188, 177–181. http://dx.doi.org/10.1016/j.envpol.2014.02.006.

Liu, Y., Chen, B., Zheng, Y., Cheng, L., Li, G., Lin, L., 2025. ODMixer: Fine-grained spatial-temporal MLP for metro origin-destination prediction. IEEE Trans. Knowl. Data Eng. 37 (9), 5508–5522. http://dx.doi.org/10.1109/TKDE.2025.3579370.

Lonsdale, J.-A., Nicholson, R., Judd, A., Elliott, M., Clarke, C., 2020. A novel approach for cumulative impacts assessment for marine spatial planning. Environ. Sci. Policy 106, 125–135. http://dx.doi.org/10.1016/j.envsci.2020.01.011.

Matplotlib Development Team, 2024. Matplotlib: Visualization with Python. Zenodo, http://dx.doi.org/10.5281/zenodo.10661079.

McDonald, R.R., Nelson, J.M., 2021. A Lagrangian particle-tracking approach to modelling larval drift in rivers. J. Ecohydraulics 6 (1), 17–35. http://dx.doi.org/10.1080/24705357.2019.1709102.

Menegon, S., Depellegrin, D., Farella, G., Gissi, E., Ghezzo, M., Sarretta, A., Venier, C., Barbanti, A., 2018a. A modelling framework for MSP-oriented cumulative effects assessment. Ecol. Indic. 91, 171–181. http://dx.doi.org/10.1016/j.ecolind.2018.03.060.

Menegon, S., Depellegrin, D., Farella, G., Sarretta, A., Venier, C., Barbanti, A., 2018b. Addressing cumulative effects, maritime conflicts and ecosystem services threats through MSP-oriented geospatial webtools. Ocean & Coastal Management 163, 417–436. http://dx.doi.org/10.1016/j.ocecoaman.2018.07.009.

Menegon, S., Sarretta, A., Depellegrin, D., Farella, G., Venier, C., Barbanti, A., 2018c. Tools4MSP: an open source software package to support maritime spatial planning. PeerJ Comput. Sci. 4, http://dx.doi.org/10.7717/peerj-cs.165.

Miladinova, S., Macias, D., Stips, A., Garcia-Gorriz, E., 2020. Identifying distribution and accumulation patterns of floating marine debris in the black sea. Marine Poll. Bull. 153, 110964. http://dx.doi.org/10.1016/j.marpolbul.2020.110964.

Mohrmann, M., C. Biddle, L., Rehder, G., Bittig, H.C., Queste, B.Y., 2025. Nord stream methane leaks spread across 14% of baltic waters. Nat. Commun. 16 (1), 281.

Nadal, I., Picciulin, M., Falcieri, F.M., García-Lafuente, J., Sammartino, S., Ghezzo, M., 2024. Spatio-temporal connectivity and dispersal seasonal patterns in the Adriatic sea using a retention clock approach. Front. Mar. Sci. 11, 1360077.

Novac, V., Moraru, L., Gasparotti, C., Rusu, E., 2020. Black Sea marine litter pollution related to naval operations. In: E3S Web of Conferences, vol. 180, EDP Sciences, p. 04018.

Özşeker, K., Coşkun, T., Erüz, C., 2024. Exploring seasonal, spatial and pathways of marine litter pollution along the southeastern black sea cost of Türkiye. Marine Poll. Bull. 202, 116348. http://dx.doi.org/10.1016/j.marpolbul.2024.116348.

Pandas development team, 2024. pandas-dev/pandas: Pandas. Zenodo, http://dx.doi.org/10.5281/zenodo.10697587.

Ricker, M., Stanev, E.V., 2020. Circulation of the European northwest shelf: a Lagrangian perspective. Ocean. Sci. 16 (3), 637–655. http://dx.doi.org/10.5194/os-16-637-2020.

Scheffer, M., Baveco, J., DeAngelis, D., Rose, K.A., van Nes, E., 1995. Super-individuals a simple solution for modelling large populations on an individual basis. Ecol. Model. 80 (2–3), 161–170. http://dx.doi.org/10.1016/0304-3800(94)00055-M.

Services using OpenDrift, 2025. https://opendrift.github.io/services.html. (Accessed: 3 Nov 2025).

Simeonova, A., Chuturkova, R., 2020. Macroplastic distribution (single-use plastics and some fishing gear) from the northern to the southern Bulgarian black sea coast. Reg. Stud. Mar. Sci. 37, 101329.

Snow, A.D., Raspaud, M., Brochart, D., Kouzoubov, K., Taves, M., Bell, R., RichardScottOZ, Chegini, T., Stefank0, Amici, A., Braun, R., Henderson, S., Annex, D.A., Brandt, C.H., Hoese, D., Bunt, F., GBallesteros, Carroll, I., Scheick, J., Hamman, J., jonasViehweger, Weidenholzer, L., Zehner, M., Cordeiro, M., Sangzi-Liang, Caldwell, S., Miller, S., The Gitter Badger, Augspurger, T., Fröhlich, Y., 2023. corteva/rioxarray: 0.15.0 Release. Zenodo, http://dx.doi.org/10.5281/zenodo.8247542.

Snow, A.D., Taves, M., BENR0, Imanol, Cook, J., SlapDrone, Abdalla, M., Pierrick, R., Bell, R., RichardScottOZ, Ji, W., 2025. corteva/geocube: 0.7.1 Release. Zenodo, http://dx.doi.org/10.5281/zenodo.14796507.

Stanev, E.V., Ricker, M., 2019. The fate of marine litter in semi-enclosed seas: a case study of the black sea. Front. Mar. Sci. 6, 660. http://dx.doi.org/10.3389/fmars.2019.00660.

Stelzenmüller, V., Rehren, J., Örey, S., Lemmen, C., Krishna, S., Hasenbein, M., Püts, M., Probst, W.N., Diekmann, R., Scheffran, J., Bos, O.G., Wirtz, K., 2024. Framing future trajectories of human activities in the German north sea to inform cumulative effects assessments and marine spatial planning. J. Environ. Manag. 349, 119507. http://dx.doi.org/10.1016/j.jenvman.2023.119507.

Stock, A., 2016. Open source software for mapping human impacts on marine ecosystems with an additive model. J. Open Res. Softw. 4 (1), 21. http://dx.doi.org/10.5334/jors.88.

Stock, A., Micheli, F., 2016. Effects of model assumptions and data quality on spatial cumulative human impact assessments. Glob. Ecol. Biogeogr. 25 (11), 1321–1332. http://dx.doi.org/10.1111/geb.12493.

Talley, L.D., 2011. Descriptive Physical Oceanography: an Introduction, Sixth ed. Academic Press, p. 560.

Terzi, Y., Gedik, K., Eryaşar, A.R., Öztürk, R.Ç., Şahin, A., Yılmaz, F., 2022. Microplastic contamination and characteristics spatially vary in the southern black sea beach sediment and sea surface water. Marine Poll. Bull. 174, 113228. http://dx.doi.org/10.1016/j.marpolbul.2021.113228.

Topçu, E.N., Tonay, A.M., Dede, A., Öztürk, A.A., Öztürk, B., 2013. Origin and abundance of marine litter along sandy beaches of the Turkish western black Sea Coast. Mar. Environ. Res. 85, 21–28.

Tsiaras, K., Hatzonikolakis, Y., Kalaroni, S., Pollani, A., Triantafyllou, G., 2021. Modeling the pathways and accumulation patterns of micro-and macro-plastics in the Mediterranean. Front. Mar. Sci. 8, 743117. http://dx.doi.org/10.3389/fmars.2021.743117.

van den Bremer, T.S., Breivik, Ø., 2018. Stokes drift. Philos. Trans. R. Soc. A: Math. Phys. Eng. Sci. 376 (2111), 20170104. http://dx.doi.org/10.1098/rsta.2017.0104.

Van Sebille, E., Griffies, S.M., Abernathey, R., Adams, T.P., Berloff, P., Biastoch, A., Blanke, B., Chassignet, E.P., Cheng, Y., Cotter, C.J., et al., 2018. Lagrangian ocean analysis: Fundamentals and practices. Ocean. Model. 121, 49–75. http://dx.doi.org/10.1016/j.ocemod.2017.11.008.

Van der Wal, M., Van der Meulen, M., Tweehuijsen, G., Peterlin, M., Palatinus, A., Kovac Viršek, M., Coscia, L., Kržan, A., 2015. Identification and assessment of riverine input of (marine) litter. Technical Report, European Commission: Bruxelles, Belgium.

Wang, X., Liu, H., Meng, X., Hu, H., 2025. GPR-FWI-Py: Open-source Python software for multi-scale regularized full waveform inversion in Ground Penetrating Radar using random excitation sources. Comput. Geosci. 197, 105870. http://dx.doi.org/10.1016/j.cageo.2025.105870, URL https://www.sciencedirect.com/science/article/pii/S0098300425000202.

Waskom, M.L., 2021. Seaborn: statistical data visualization. J. Open Source Softw. 6 (60), 3021. http://dx.doi.org/10.21105/joss.03021.

Willsteed, E.A., Birchenough, S.N.R., Gill, A.B., Jude, S., 2018. Structuring cumulative effects assessments to support regional and local marine management and planning obligations. Mar. Policy 98, 23–32. http://dx.doi.org/10.1016/j.marpol.2018.09.006.

Zambianchi, E., Trani, M., Falco, P., 2017. Lagrangian transport of marine litter in the Mediterranean sea. Front. Environ. Sci. 5, 5. http://dx.doi.org/10.3389/fenvs.2017.00005.

Zancanaro, M., Mulazzani, A., Barbanti, A., Menegon, S., 2025. Design Thinking and Maritime Spatial Planning: similarities, differences and opportunities for design. In: Proceedings of the 16th Biannual Conference of the Italian SIGCHI Chapter. CHItaly '25, Association for Computing Machinery, New York, NY, USA, http://dx.doi.org/10.1145/3750069.3750084.

Zhong, Z., Burhan, M., Ng, K.C., Cui, X., Chen, Q., 2024. Low-temperature desalination driven by waste heat of nuclear power plants: A thermo-economic analysis. Desalination 576, 117325.